Simulation of the Cryogenic Behavior

of the Superconducting Magnets

in the Energy Saver

Judith E. Nicholls, Henry R. Barton

and George T. Mulholland

April 20, 1981

Abstract

A time-dependent model of the Energy Saver cryoloop has been developed to simulate the cryogenic behavior of the superconducting magnets. Preliminary results include temperature, pressure, enthalpy, and velocity distributions. These calculations are reported for steady-state conditions, and transient behavior during accelerator ramping and ramp-off. Transient effects on beam storage operation require further work.

Introduction

A Satellite refrigerator provides cooling to two parallel 20-magnet cryoloops. A single cryoloop is modeled with one-half Satellite flow; Fig. 1 shows the relationship of these parts of the system. Fig. 2 diagrams the 20-magnet string modeled here. Liquid helium flows to the magnet string through a subcooler at 1.8 atm, and is expanded at the far end to a lower pressure to return as two-phase liquid. The ramping heat load is deposited in the single-phase stream and is transferred to the colder two-phase counter-flow stream. The heat is primarily absorbed by the heat of vaporization of the two-phase fluid that returns to the Satellite through the shell side of the subcooler.

Model

The cryoloop was simulated by simultaneous numerical solution of the one-dimensional mass, energy, and momentum conservation equations describing the helium streams, subject to appropriate boundary and initial conditions. The method follows that used by M. C. Jones[1] on the counterflow cooldown of superconducting power transmission lines, and uses the computer program PDECOL developed by N. K. Madsen and R. F. Sincovec[2] to integrate the partial differential equations.

PDECOL solves a set of three equations for each stream: the one-dimensional conservation equations written in terms of pressure P, enthalpy H, and velocity V.[3]

$$\frac{\partial P}{\partial t} = -V\frac{\partial P}{\partial X} - c^2\frac{\partial V}{\partial X} + \phi\left[\frac{\Lambda}{a} + \rho\frac{V^2 f|V|p}{2a}\right]$$

$$\frac{\partial H}{\partial t} = -V\frac{\partial H}{\partial X} - c^2\frac{\partial V}{\partial X} + \left(\frac{1+\phi}{\rho}\right)\left[\frac{\Lambda}{a} + \rho\frac{V^2 f|V|p}{2a}\right]$$

$$\frac{\partial V}{\partial t} = -\frac{1}{\rho}\frac{\partial P}{\partial X} - V\frac{\partial V}{\partial X} - \frac{f V|V|p}{2a}$$

We have eliminated the space and time derivatives of the density ρ in the mass conservation equation using

$$d\rho = \left(\frac{\partial \rho}{\partial H}\right)_P dH + \left(\frac{\partial \rho}{\partial P}\right)_H dP$$

We still must know the density as a function of P and H as well as its derivatives with respect to P and H. The equations are simplified by writing them in terms of the Gruniesen parameter ϕ and the acoustic velocity c:

$$c^2 = 1/(\ (\partial \rho/\partial P)_H + \frac{1}{\rho}(\partial \rho/\partial H)_P\ )$$

$$\phi = -\frac{c^2}{\rho}\left(\frac{\partial \rho}{\partial H}\right)_P$$

The necessary helium properties are parametrized as functions of P and H.[4]

Λ is the heat transfer to the fluid per unit length. These sets of equations are effectively coupled through the heat transfer equation (which is discussed below) and the boundary conditions.

The friction factor is f, and p and a the wetted perimeter and cross-sectional area of the channel. The Cryoloop Simulation parameter list is included as Appendix I.

The model is spatially uniform; the overall cross-sectional area, perimeter, heat inputs, and heat transfer coefficient are independent of x. The active portions of the magnet string have been modeled, i.e., the effective length used here neglects the magnet interconnections.

The boundary conditions selected fix the pressure of both streams and the enthalpy of the single-phase stream at the refrigerator end (x=0). The mass flow is fixed at the valve and the mass and enthalpy are continuous across it. The mass flow is chosen so that the fluid is 10% liquid at the exit. The model makes no provision for power or correction lead flows, but includes heat leak due to the power leads.

Initial conditions (t=0) must be provided for all values of x. The program is required to converge to a good steady state solution ($\partial(\ )/\partial t \to 0$) as a starting point for the time-dependent studies.

The heat transfer to the fluid, Λ , is composed of two parts: the static load from heat leaks and the ramping load. At each spatial and temporal point, the heat transfer Λ is calculated from the external heat applied to each stream and the heat transfer from the single-phase to the two-phase stream. This stream-to-stream heat transfer is proportional to the temperature difference between the two streams and the heat transfer coefficient, which is a function of the geometry and materials. Although this coefficient does have some flow dependence, the average value used here provides a good approximation for the flow studied.

The equation used for the heat transfer per unit length is

$$Q_T = p_1 \cdot h_{tr} \cdot (T1-T2)/2$$

where p_1 is the total wetted perimeter of stream 1, and h_{tr}, the heat transfer coefficient, was taken to be 3.35 mW/cm^2-$^\circ$K.[5]

In this paper P1, H1, and V1 refer to the single-phase stream and P2, H2, and V2 refer to the two-phase stream. Similarly, T1 and T2 refer to the temperatures, and R1 and R2 refer to the densities of the streams.

Steady State

A steady state case has been solved for an average
anticipated load: average dynamic load of 250 watts, 10
watts heat leak into the single-phase stream, and 140 watts
of heat leak directly into the 2-phase stream.

The boundary conditions at x=0 are
H1 = 11.43 j/g
P1 = 1.8 atm
P2 = 1.209 atm

The boundary conditions at x=L are
$V1 = \dot{M}/R1 \cdot a_1$ where $\dot{M}$ = 23.81 g/sec, R1 is the density of
stream 1 at x=L, and a_1 is the cross sectional area of
stream 1 (19.8 cm^2).
H1 = H2
$\dot{M}_1 = V1/R1 \cdot a_1 = \dot{M}_2 = V2/R2 \cdot a_2$ where R2 is the density of
stream 2 at x=L and a_2 is the cross sectional area of
stream 2 (11.255 cm^2).

Fig. 3 shows T1, the temperature of stream 1, T2, the
temperature of stream 2, and Q_T, the heat transferred from
stream 1 to stream 2 as a function of the distance along the
magnet string.

Notice that x=0 is the inlet and x=L the turnaround.

Figs. 4 and 5 show the pressures of the two streams as
functions of x. The densities, R1 and R2, are shown in
Figs. 6 and 7. R1 shows the simple effects of increasing
temperature. R2 reflects the increasing proportion of gas
from x=L to x=0. The velocities of the fluid, V1 and V2,
are shown in Figs. 8 and 9, and the enthalpies, H1 and H2,
in Figs. 10 and 11.

Ramping

The ramping current can be any I(t) for which Q(t)=F(I(t))
is known. The ramp model used (200 A/sec, I_{max}=4000 A, 5
sec flat top and 60 sec cycle time) closely parallels
anticipated ramping (Fig. 12). The load is taken to be
proportional to $(\partial B/\partial t)^n$ and modified to one second rise and
fall times for computational convenience. The resultant
trapezoidal wave form has a peak of 375 W and an average of
250 W. The heat leak is the same as the steady state case.

The ramp is turned on to the steady state solution. The boundary conditions are the same as the steady state.

The effect of ramping on the temperature is shown in Fig. 13 at x=0, L, and L/2 for two ramp cycles and both streams. Large values of $\partial(T1)/\partial t$ have correspondingly large $\partial(R1)/\partial t$ that provide velocities of expansion and contraction that subtract from, and add to, the transport velocity. The velocities of the streams at x=0, L, and L/2 are shown in Figs. 14 and 15. Fixing the flow rate at the valve results in large variations at the refrigerator.

Figs. 16 and 17 show the pressures as a function of t at x=0, L/2; and L; Figs. 18 and 19, the enthalpies; and Figs. 20 and 21, the densities.

Ramp Off

The Saver Operations Group empirically demonstrated a cryoloop upset behavior caused by suddenly turning the full ramp off. Under the controls appropriate to the steady state, a dramatic flow imbalance is observed at the refrigerator and it warms up significantly at its cold end. The magnet simulator was tested, in a preliminary way, to study that situation. The 250 watt steady state dynamic load was reduced to 10 watts in one second, and the boundary conditions held to approximate the "frozen" controls on ramp-off that are now in effect.

The temperature distributions as a function of x at 20 second intervals are shown in Figs. 22 and 23. The t=0 curves correspond to the steady state temperature distribution (see Fig. 3). Figs. 24 through 32 show the behavior of the other quantities as a function of x at 20 second invervals.

The velocities of the single-phase stream at x=0, L/2, and L are shown in Fig. 33 as a function of time for 1200 seconds. The velocities rise instantaneously, greater the nearer the inlet, from values that were nearly equal (to within a few percent) at t=0. The effect is brought about by the rapid rise in single-phase fluid density in the absence of a heat load. As the stream-to-stream ΔT decays, the effect subsides.

The behavior of the single-phase stream as a function of time, odd-numbered Figs. 33 to 41, describe the situation very well at small t. The actual behavior deviates from

that simulated as t grows larger because of the assumption of constant mass flow. The demand for liquid of the single-phase stream (up to 300 l/hr) at ramp-off cannot be provided by the current refrigerator. The instantaneous peak for the whole Saver would be 48 x (300 l/hr) = 14,400 l/hr.

The behavior of the two-phase stream, even-numbered Figs. 34 through 42, is a good description through the first tens of seconds. The enthalpy, H2, Fig. 40, makes it clear that the liquid fraction is increasing dramatically, especially at the exit (x=0), after the sharp reduction in load. The real situation differs in two respects at large t: first, the assumption of constant mass flow fails as before, and, second, the integrated effect, the collection of liquid, is enhanced by continued inactivity of the valve.

This indication of the magnitude of the transient behavior has suggested hardware modifications aimed at significantly reducing the effects. These considerations are properly the subject of a paper themselves and are mentioned here in support of the continued development of this work. Ramp-off will, unavoidably, be frequently exercised in the early trials and the cryoloop should be prepared to deal with its consequences. It should be noted that the transition from ramping to extended flat-top, beam coasting, or beam storage mode are different from the ramp-off transient only in the instantaneous ramp rate and the recent ramp history. Item 4 of the work agenda address this concern.

Future Work

Although the work is far from complete, we felt an interim report should be distributed to establish capability, direction, and to solicit comments.

The agenda of work currently is to

1) develop a no-ramp-load steady state,

2) apply the ramp to this steady state (i.e., saver turn-on) at various rates,

3) turn the ramp off,

4) from the steady state in item 1, ramp up, then simulate beam storage with flat-tops of various lengths,

5) install two-phase superheat feedback to a mass flow control valve and test the ramp-off behavior.

References

1 Jones, M.C., "Cool-down of superconducting power transmission lines with single phase helium," Cryogenics, March 1980, p 139.

2 Madsen, N.K., Sincovec, R.F. in Numerical Methods for Differential Systems, L. Lapidus, W. E. Shiesser, ed. (Academic Press Inc., New York, 1976).

3 Arp, V., "Thermodynamics of single-phase one-dimensional fluid flow," Cryogenics, May 1975, p 285.

4 Arp, V., N.B.S., Boulder, Colo., private communication.

5 Mulholland, George, Magnet Heat Transfer, Fermilab Memo, June 25, 1980.

APPENDIX I

APRIL 1981

		PARAMETER LIST: CRYOLOOP SIMULATION	VALUE
CHL	1.	CHL FEED ENTHALPY (J/G), $N = 0$	12.33
	2.	CHL FEED ENTHALPY (J/G), F(N) (SEE NOTE 1)	$P1 + \Delta H_2$
	3.	CHL PRODUCTION RATE (G/S).	139
	4.	FRACTION OF CHL PRODUCTION UTILIZED, X	0.9
LN_2	5.	LN_2 FEED ENTHALPY (J/G), $N = 0$	34.8
	6.	LN_2 FEED ENTHALPY (J/G), F(N) (SEE NOTE 2)	$P5 + \Delta H_5$
	7.	LN_2 FEED PRODUCTION RATE (G/S)	568
	8.	FRACTION OF LN_2 PRODUCTION UTILIZED, Y	0.9
LINES	9.	TOTAL HEAT LEAK LHE TRANSFER LINE (J/S).	300
	10.	TOTAL HEAT LEAK LN_2 TRANSFER LINE (J/S).	4500
COMP.	11.	TOTAL RING COMPRESSOR FLOW (G/S)/24 (NOMINAL)(SEE NOTE 3).	50
	12.	SUCTION MANIFOLD PRESSURE (ATM).	1.03
	13.	DISCHARGE MANIFOLD PRESSURE (ATM).	20.0
	14.	DISCHARGE TEMPERATURE (°K)	316
LEADS	15.	DIPOLE LEAD FLOW TOTAL (G/S)	0.48
	16.	CORRECTION LEAD FLOW TOTAL (G/S)	0.48
	17.	DIPOLE LEAD MAXIMUM RAMP HEAT LEAK TOTAL	10
	18.	CORRECTION LEAD HEAT LEAK TOTAL	10
REFRIG.	19.	CRYOLOOP REFRIGERATOR NUMBER, N	24
&	20.	STATIC HEAT LEAK (@5-6°K), REFRIG. (J/S)	10
ENGS.	21.	STATIC HEAT LEAK, GAS ENGINE (J/S)	10
	22.	GAS ENGINE DISPLACEMENT (CM³).	463
	23.	MAXIMUM GAS ENGINE SPEED (RPM)	317
	24.	MINIMUM GAS ENGINE SPEED (RPM)	120

CONT'D.

PARAMETER LIST: CRYOLOOP SIMULATION (CONT'D.)   <u>VALUE</u>

25. EFFICIENCY GAS ENGINE 0.65

26. INTAKE CUT-OFF ENGINE 0.38

27. STATIC HEAT LEAK WET ENGINE (J/s) 16

28. WET ENGINE DISPLACEMENT (CM³) 206

29. WET ENGINE MAXIMUM SPEED (RPM). 317

30. WET ENGINE MINIMUM SPEED (RPM). 107

31. EFFICIENCY OF WET ENGINE (NOMINAL). 0.7

32. INTAKE CUT-OFF WET ENGINE 0.7

33. SHELL SIDE PRESSURE DROP (ATM). 0.195

34. TUBE SIDE PRESSURE DROP (ATM) . . . . 1.0 ^{TYP}

35. SINGLE PHASE SOURCE PRESSURE (ATM). 1.8

36. 2Ø RETURN PRESSURE (ATM), P12+P33 . . . . 1.23 TYP

37. HEAT EXCHANGER CAPACITY (W/°K), (M/40)$^{0.8}$(1.4×10⁴) 1.67E4

SUB-   ⊤ 38. SINGLE PHASE SOURCE TEMPERATURE (°K). . . . . 4.5 TYP

COOLER   39. SUPER HEAT OF 2Ø RETURN (°K) . . . . 0.1 TYP

40. SUBCOOLER TEMPERATURE APPROACH (°K) 0.09

41. SUBCOOLER RESERVOIR VOLUME (CM³). 10E3

MAG.   ⊤ 42. NUMBER OF DIPOLES IN CRYOLOOP 16

HALF   43. NUMBER OF QUADRUPOLES IN CRYOLOOP 4

STRING   44. STATIC HEAT LEAK/DIPOLE (J/s) 7

45. STATIC HEAT LEAK/QUADRUPOLE (J/s) 7

46. HALF TOTAL OF OTHER STRING HEAT LEAKS (J/s) 20

47. 1Ø DIPOLE CROSS SECTIONAL AREA (CM²), 7.58+12.22 . . . . . . 19.8

48. 2Ø DIPOLE CROSS SECTIONAL AREA (CM²). 11.3

49. 1Ø QUADRUPOLE CROSS SECTIONAL AREA (CM²), 17.3+7.20. . . . . 24.5

50. 2Ø QUADRUPOLE CROSS SECTIONAL AREA (CM²). 16.5

51. 1Ø DIPOLE WETTED PERIMETER (CM) 119.3

CONT'D.

PARAMETER LIST: CRYOLOOP SIMULATION (CONT'D.) VALUE

52. 2Ø DIPOLE WETTED PERIMTER (CM) 87.9

53. 1Ø QUADRUPOLE WETTED PERIMETER (CM), 50.2+95.7. 146

54. 2Ø QUADRUPOLE WETTED PERIMETER (CM), (ESTIMATE) 90

55. DIPOLE LENGTH (CM) 608

56. QUADRUPOLE LENGTH (CM) 175

57. SUBCOOLER-LHe ENGINE POTENTIAL (CM). 914

58. RAMPING LOAD, AVERAGE (J/s) 240

59. FRICTION FACTOR 1Ø 5.26E-3

60. FRICTION FACTOR 2Ø AVERAGE 4.45E-3

61. LOCAL ATMOSPHERIC PRESSURE (A_s). 0.973

62. HEAT TRANSFER COEF. (WINDING TO 2Ø) MW/CM°K. . . . . 3.35 TYP

NOTES:

1. $$\Delta H_2 = \sum_{i=0}^{i=N} \frac{P9}{(24-i(P4))(P3)}$$

2. $$\Delta H_5 = \sum_{i=0}^{i=N} \frac{P10}{(24-i(P8))(P7)}$$

3. MASS DEPENDENT PARAMETER VALUES ARE PROVIDED AT THE FLOW RATE OF PARAMETER 11.

TM-1042
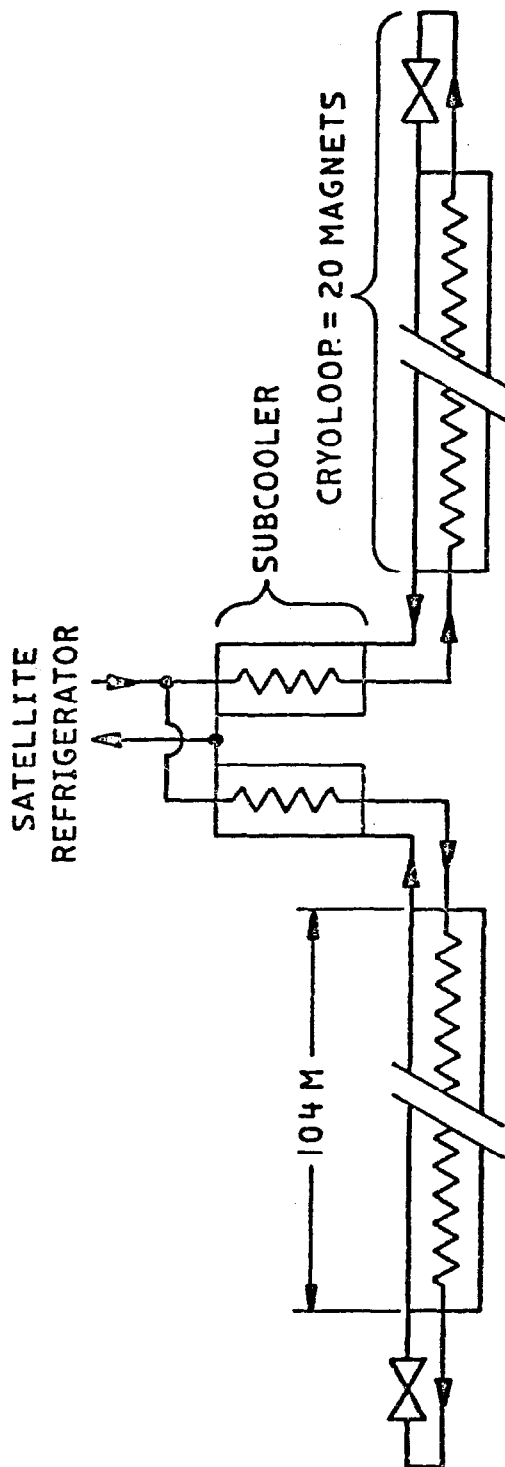
Figure 1. A Satellite drives parallel cryoloops.
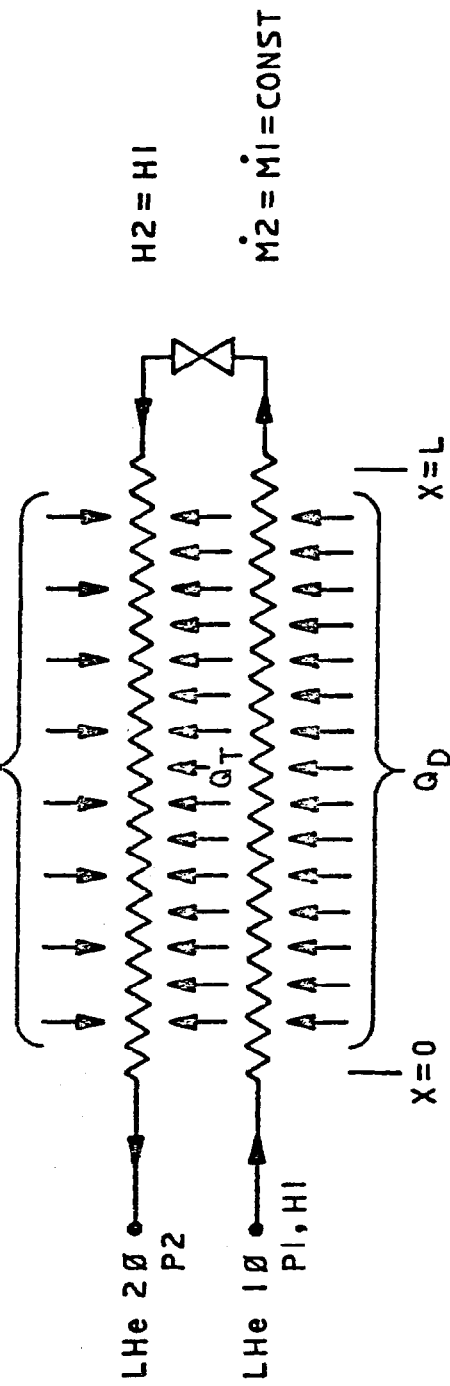
Figure 2. A cryoloop as a distributed heat exchanger.
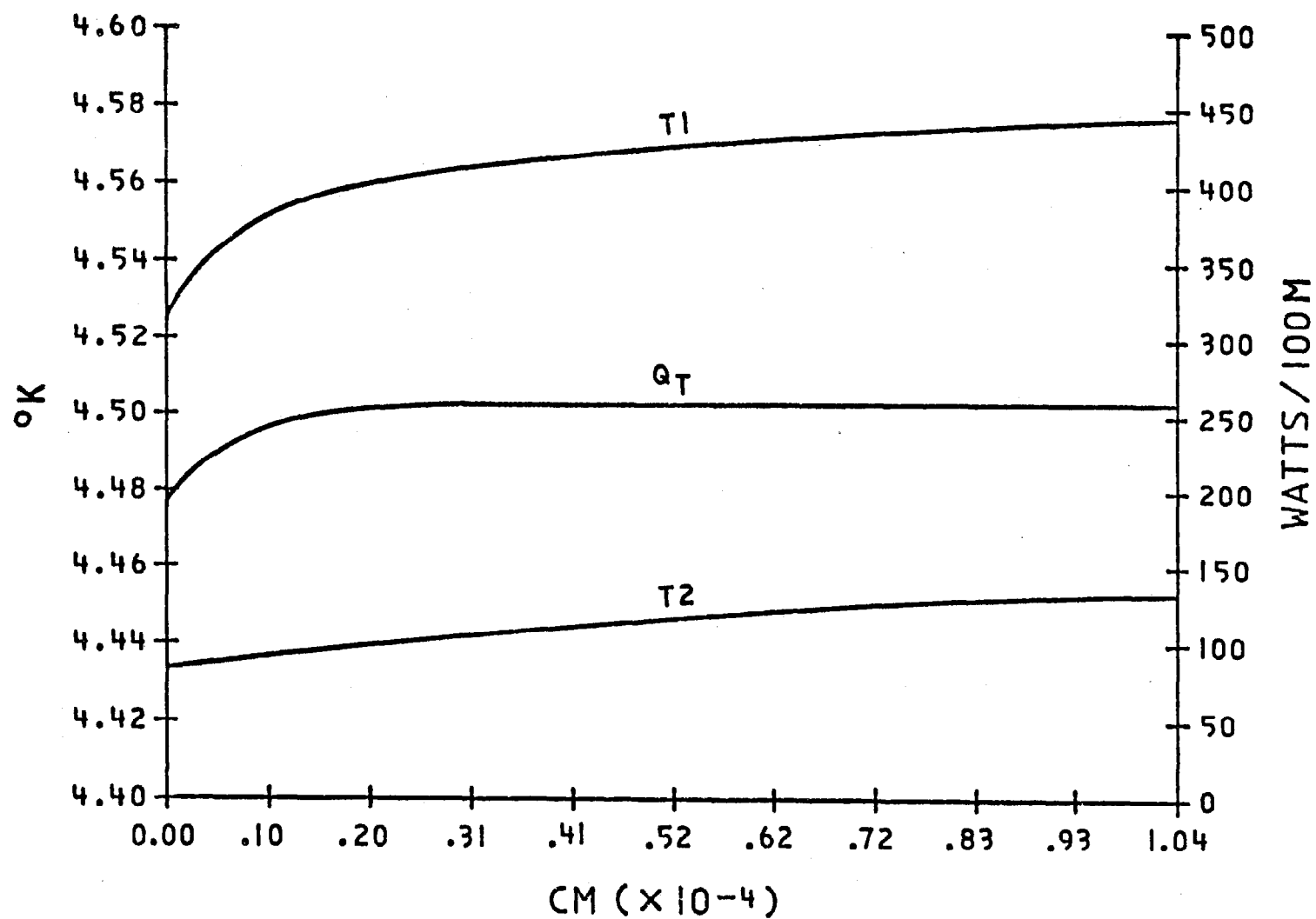
Figure 3.   Temperatures and heat transfer of steady state (DC) mode.
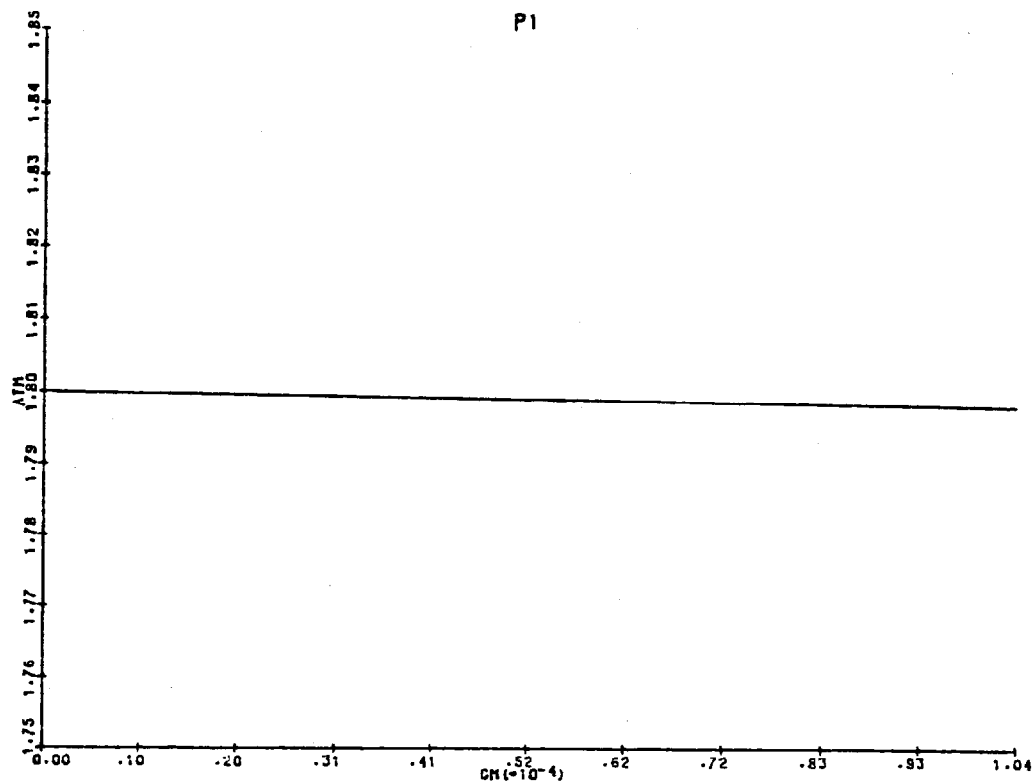
Figure 4.   Pressure of single-phase stream as a function of x.
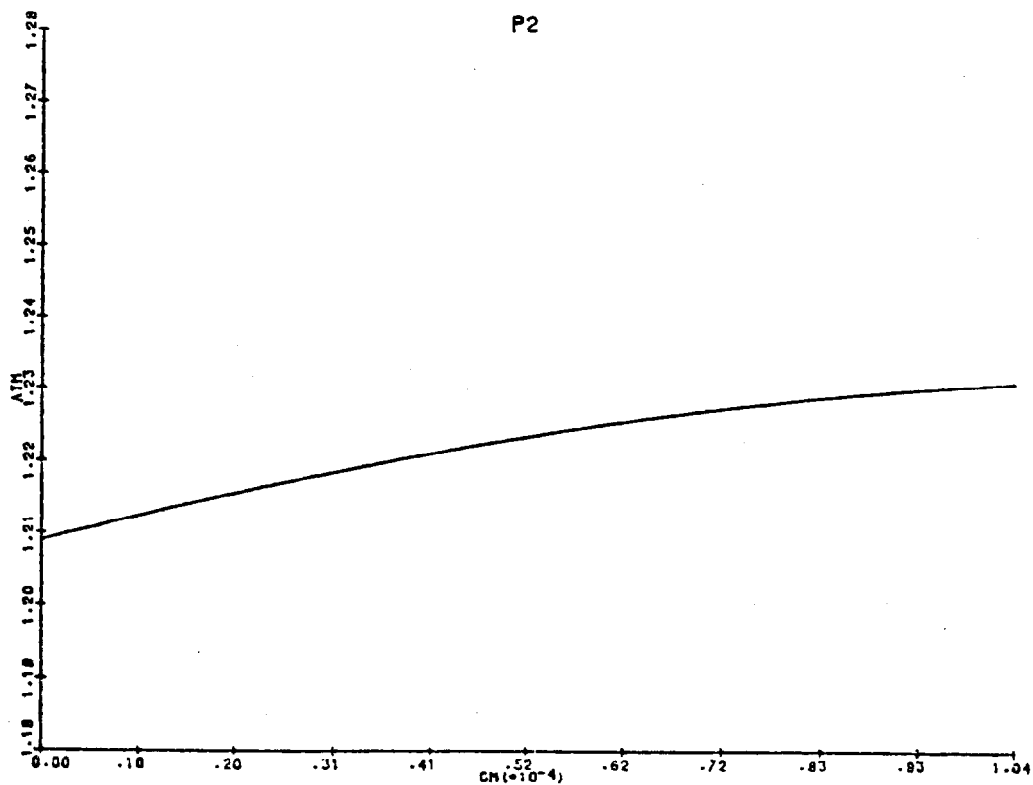
Figure 5.   Pressure of the two-phase stream as a function of x.
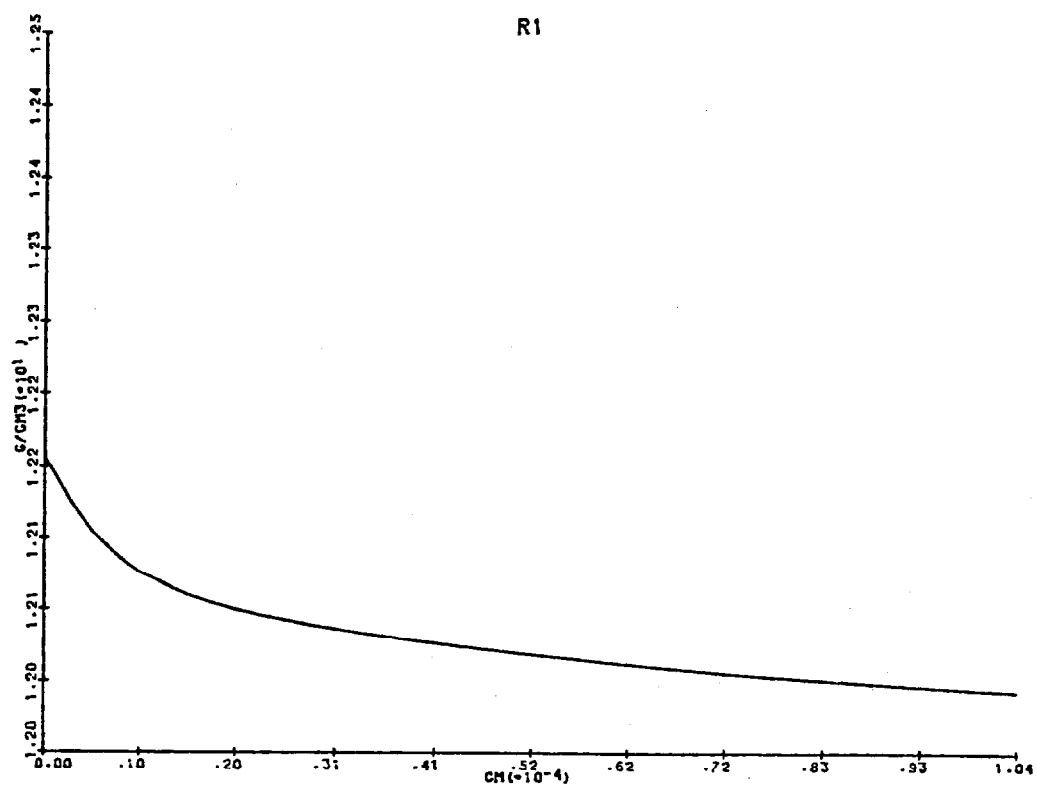
Figure 6. Density of single-phase stream as a function of x.
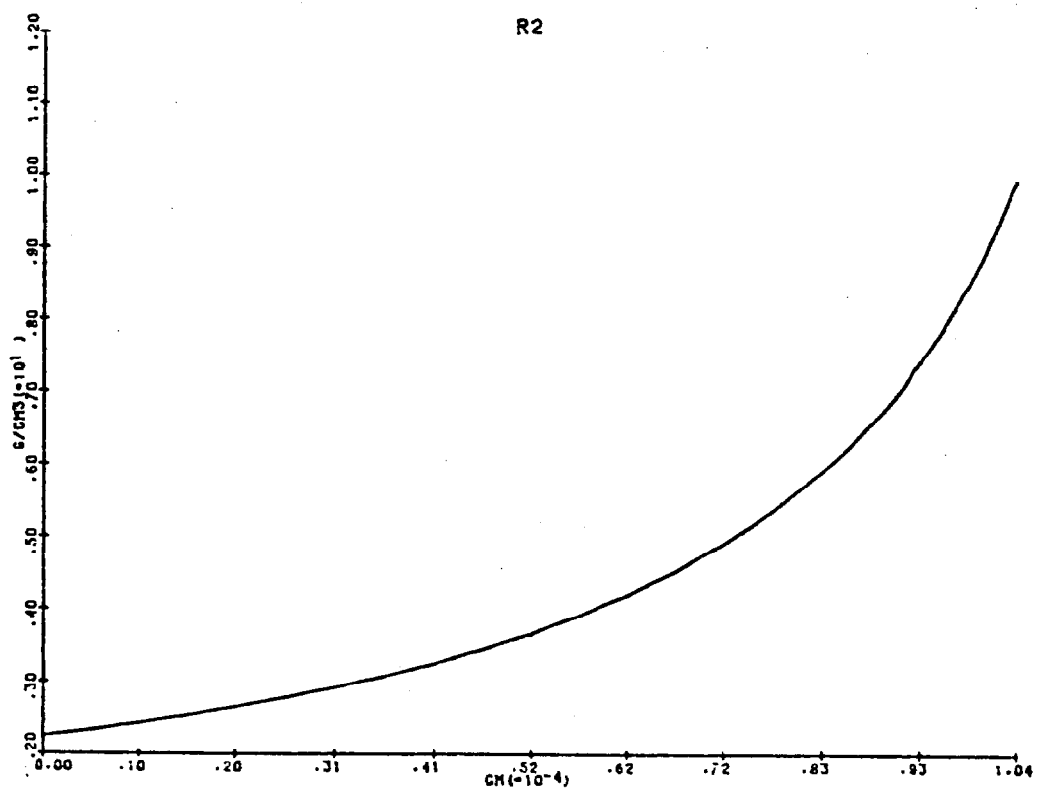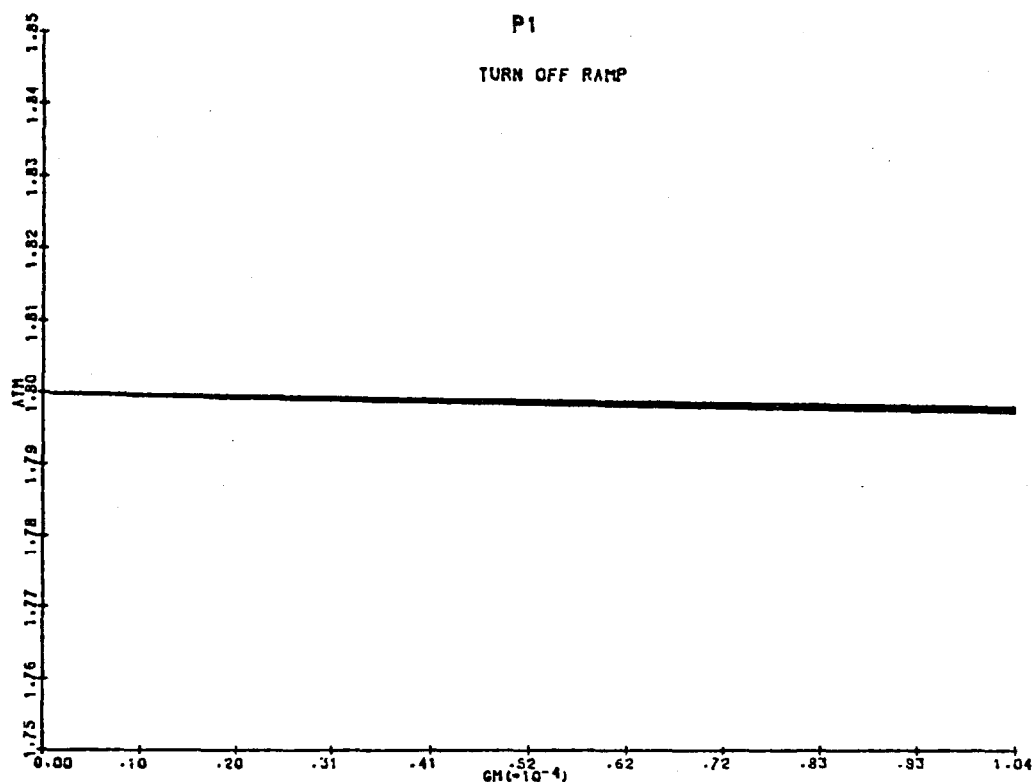

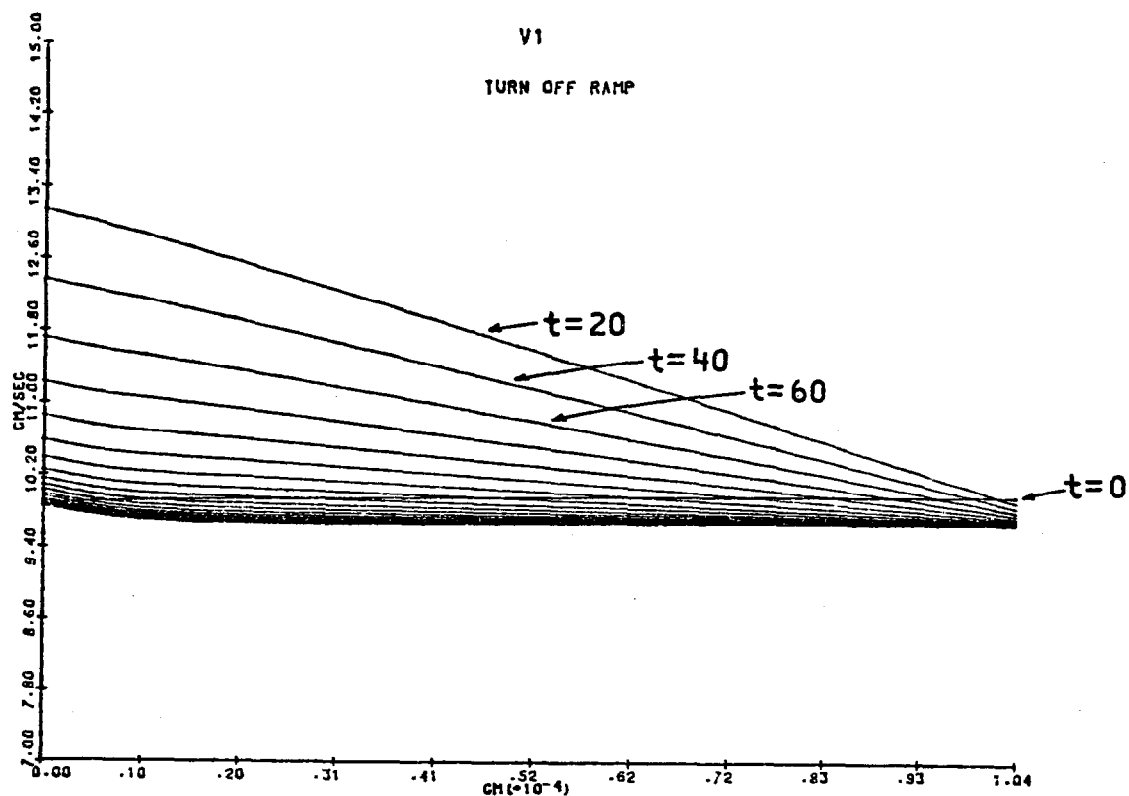Figure 7. Density of two-phase stream as a function of x.

V1

CM/SEC

CM(*10⁻⁴)
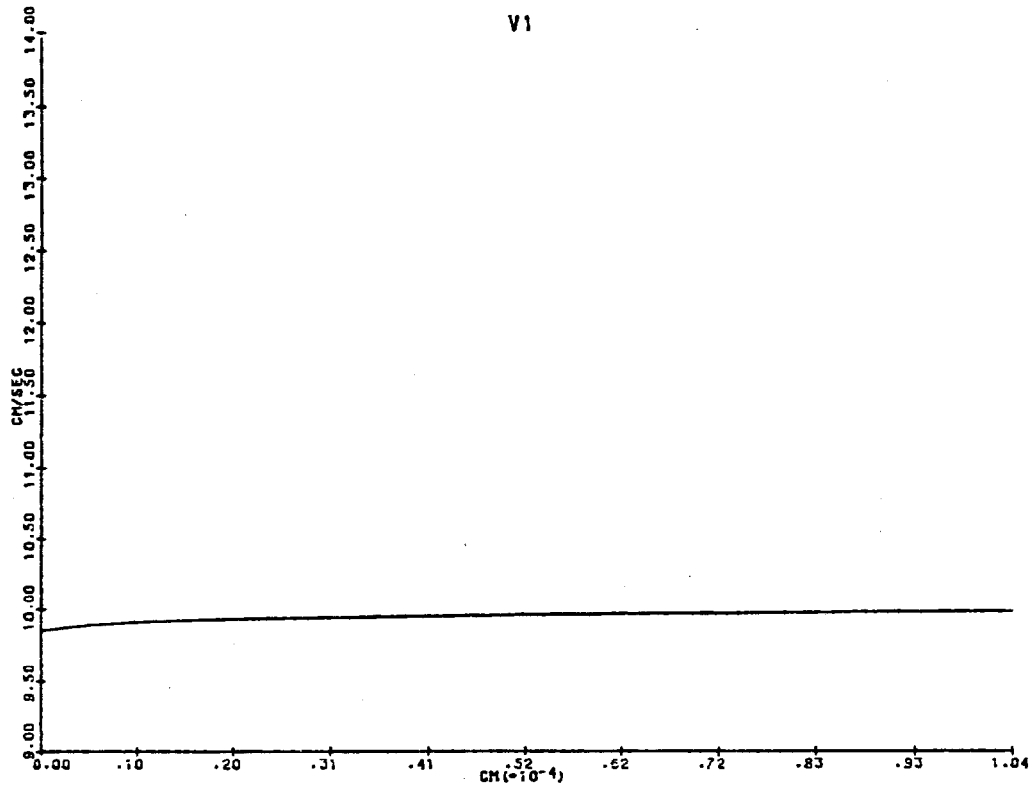
Figure 8. Velocity of single-phase stream as a function of x.

V2

CM/SEC

CM(*10⁻⁴)
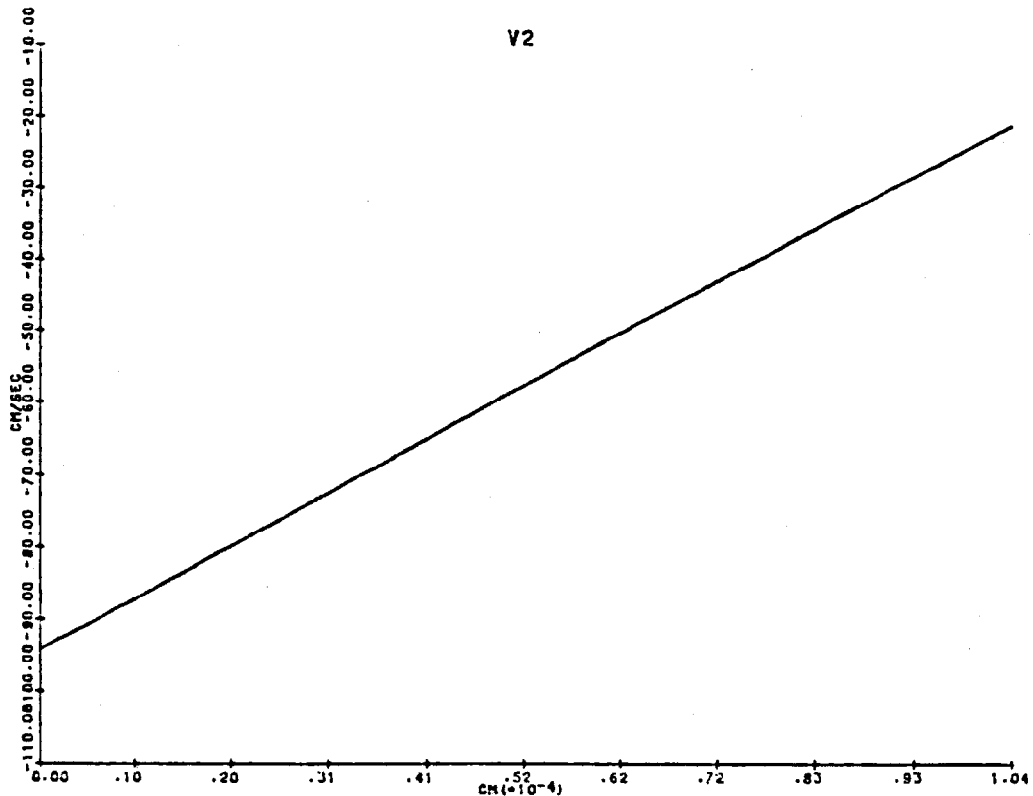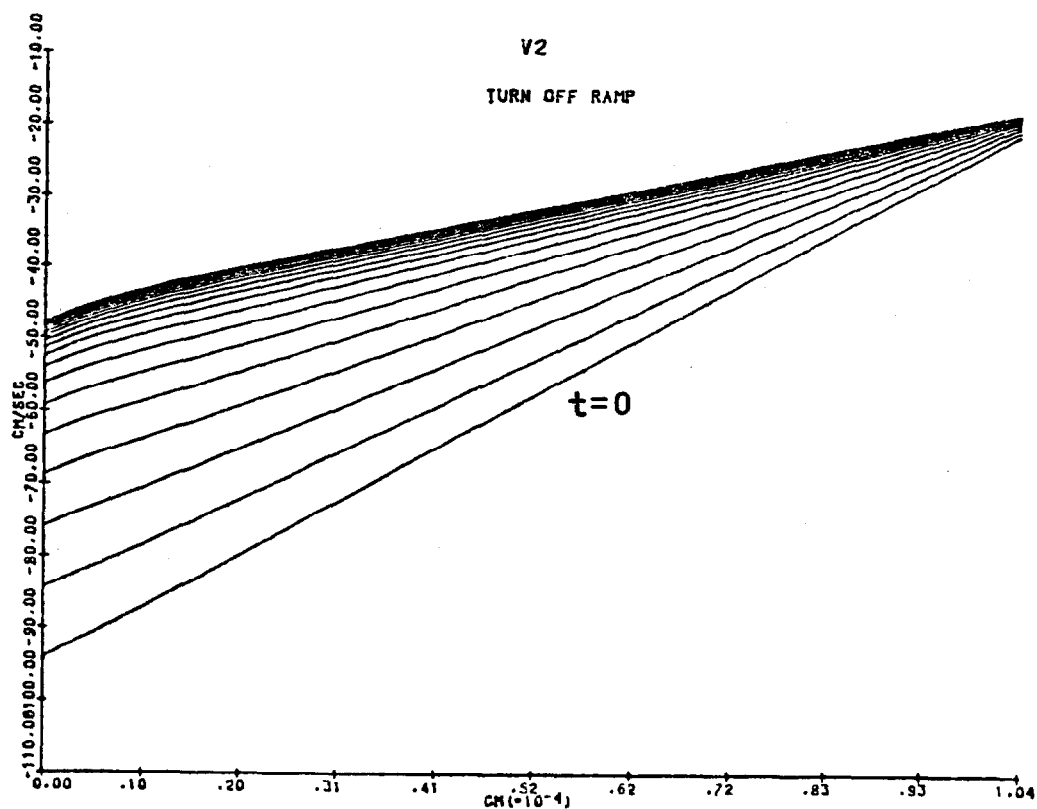
Figure 9. Velocity of two-phase stream as a function of x.
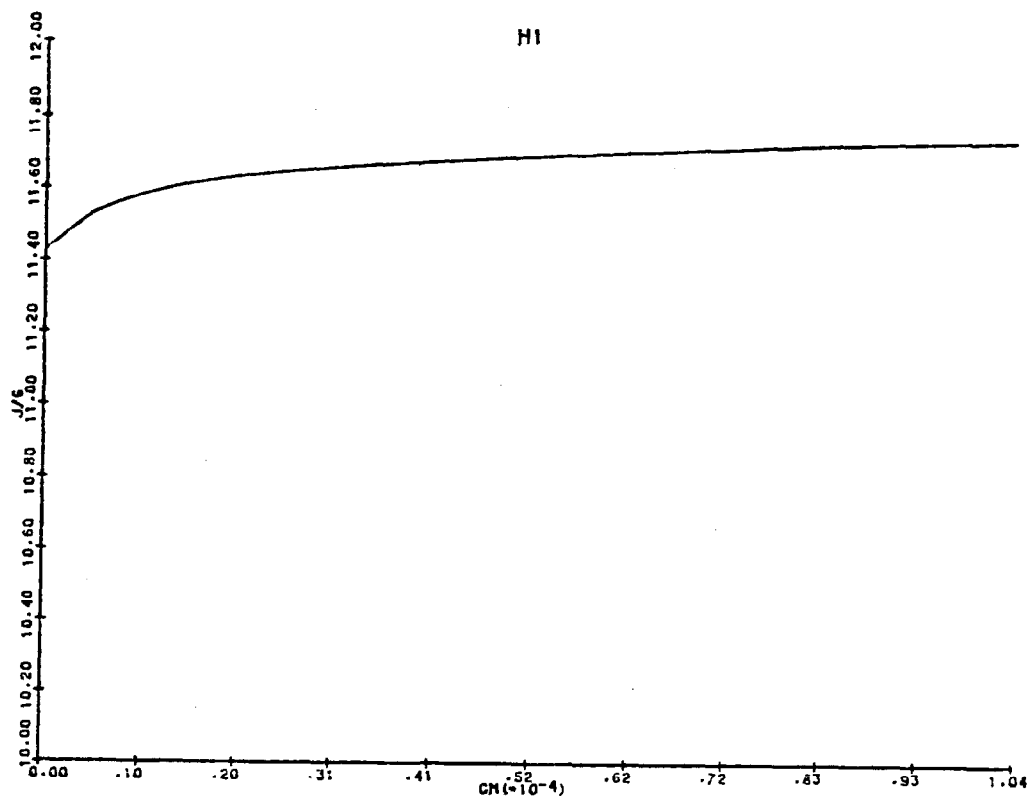
Figure 10.   Enthalpy of single-phase stream as a function of x.
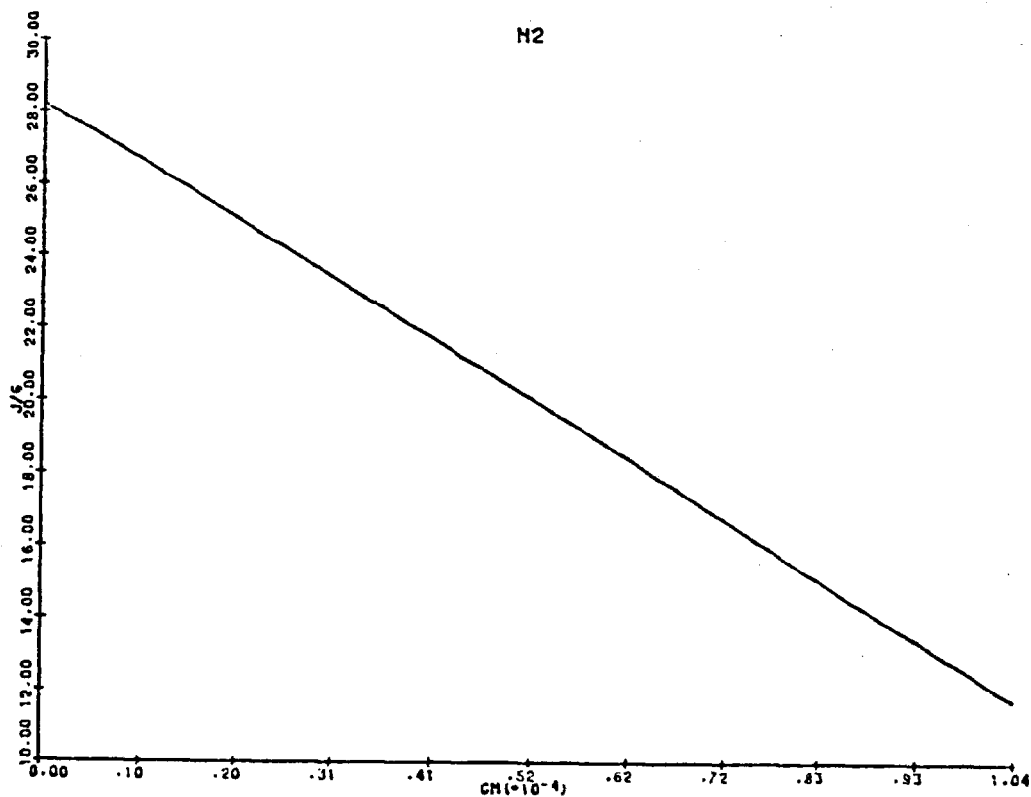
Figure 11.   Enthalpy of two-phase stream as a function of x.
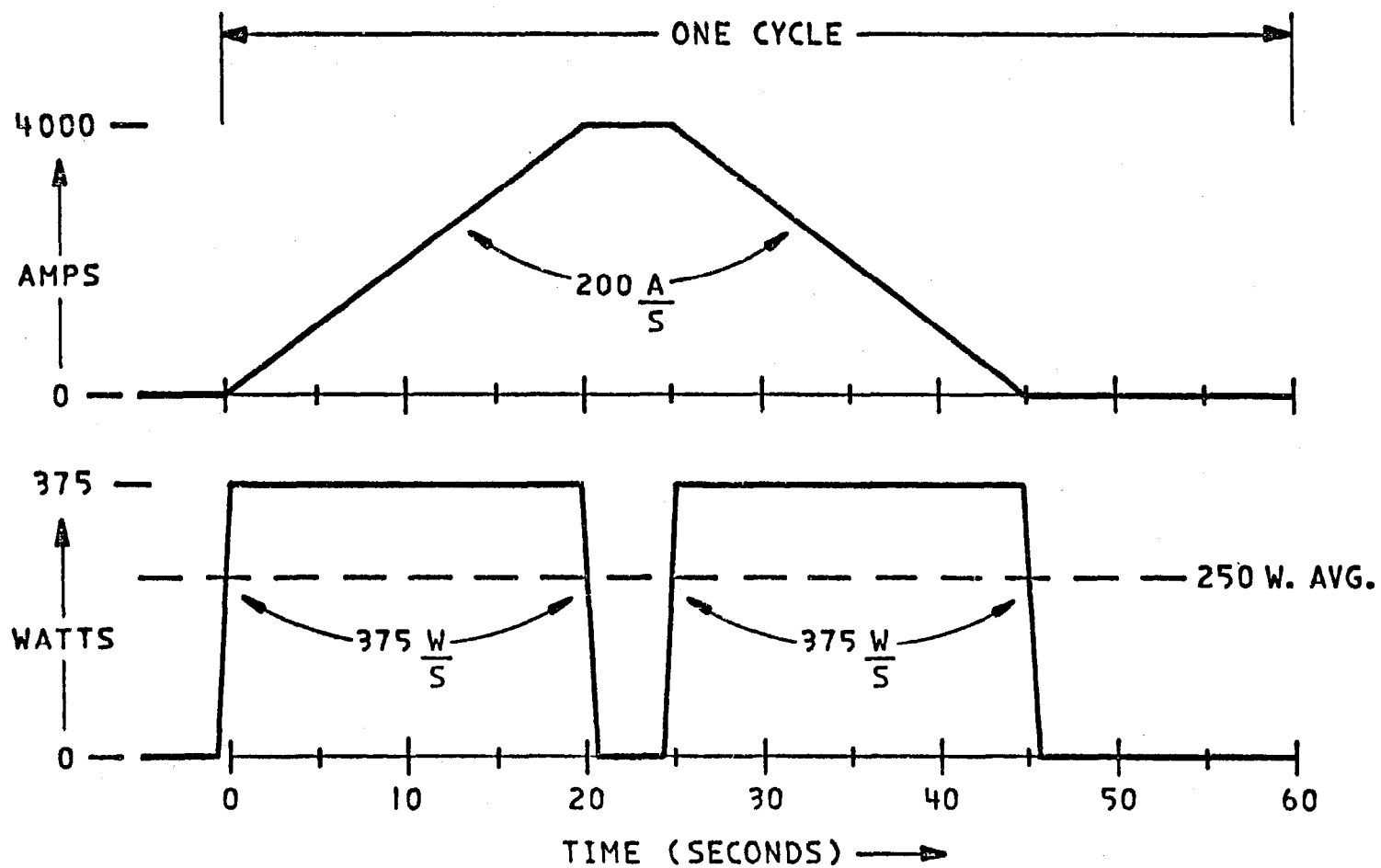
Figure 12.   Assumed ramping current and refrigeration load as a function of time.
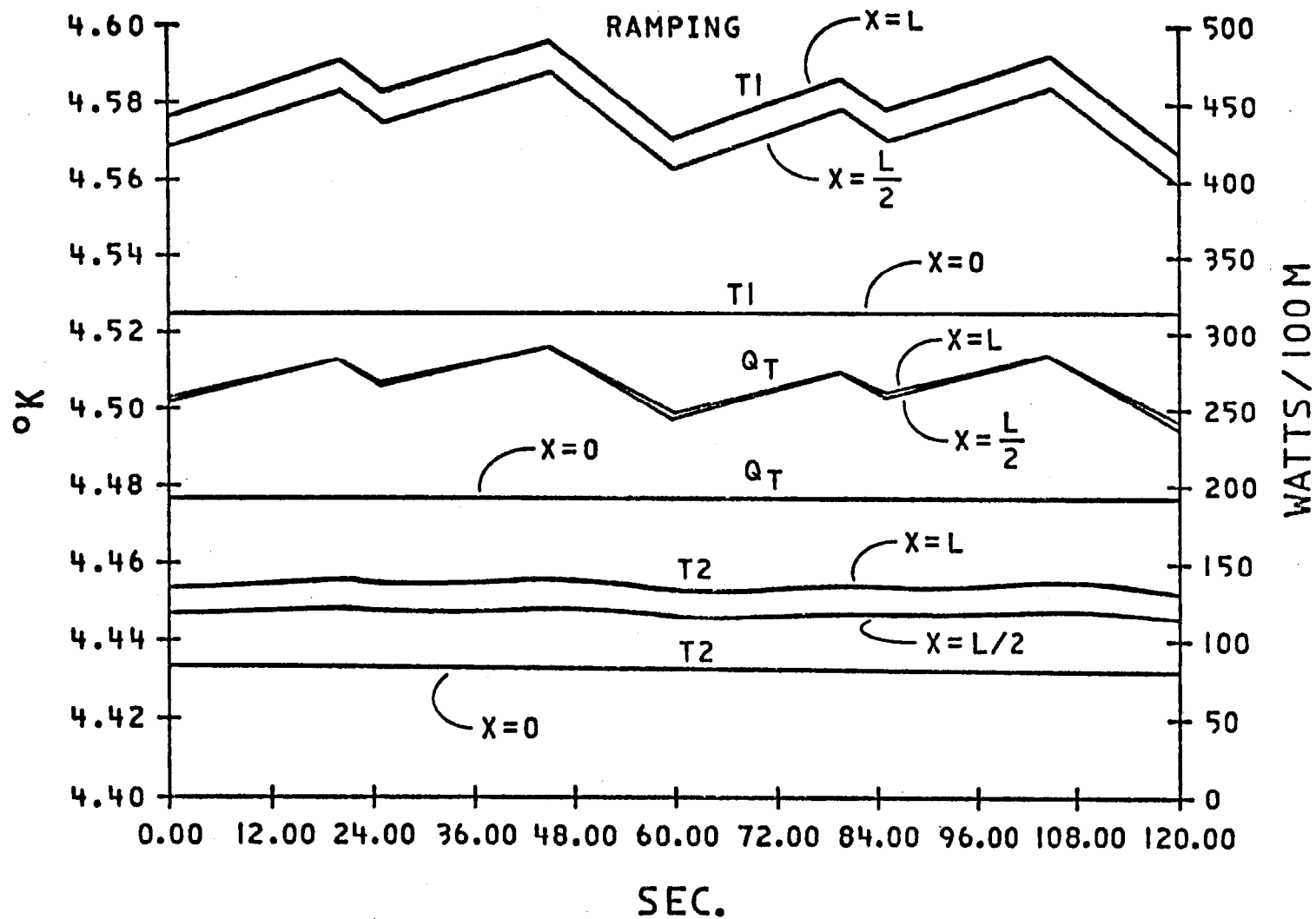
Figure 13; Heat transfer and single- and two-phase temperatures for two ramp cycles.
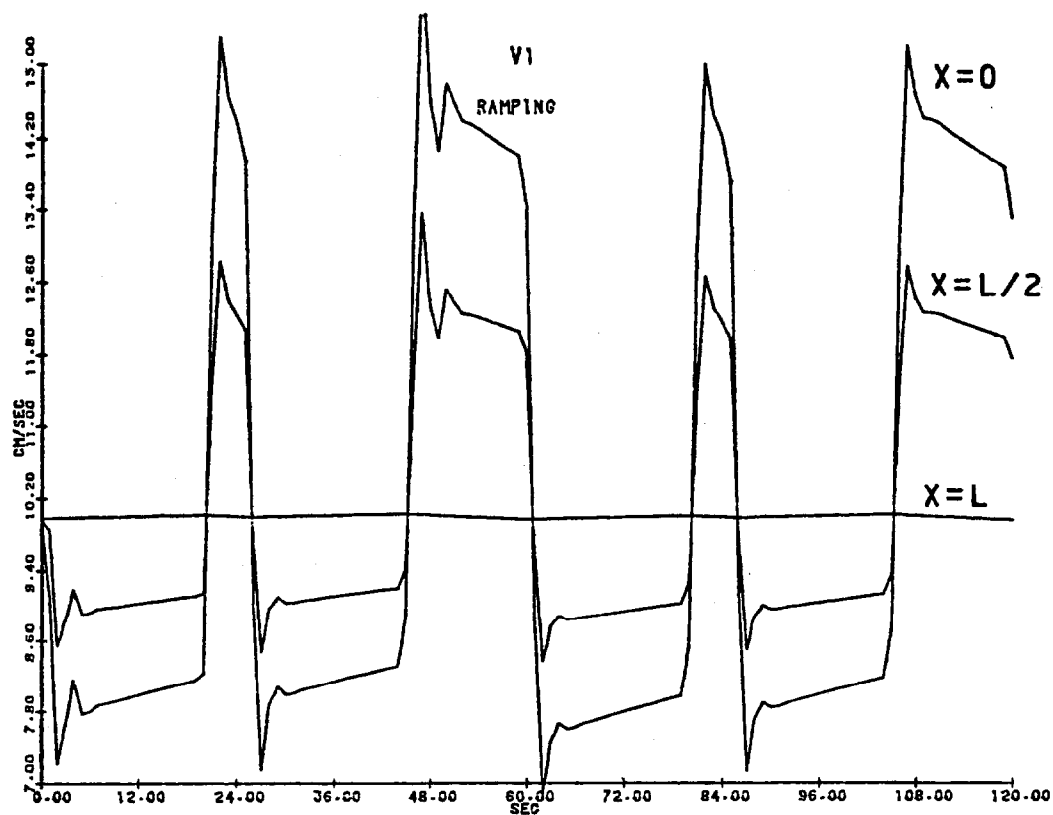
Figure 14. Velocity of single-phase stream over two ramp cycles.
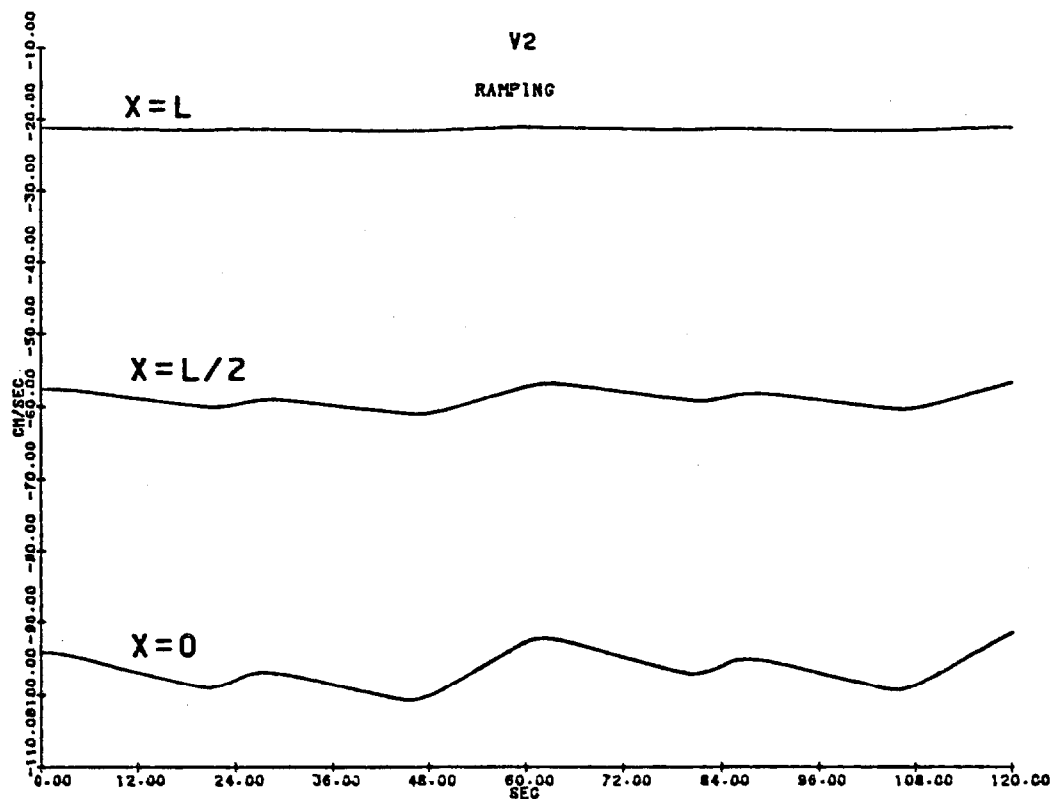
Figure 15. Velocity of two-phase stream over two ramp cycles.
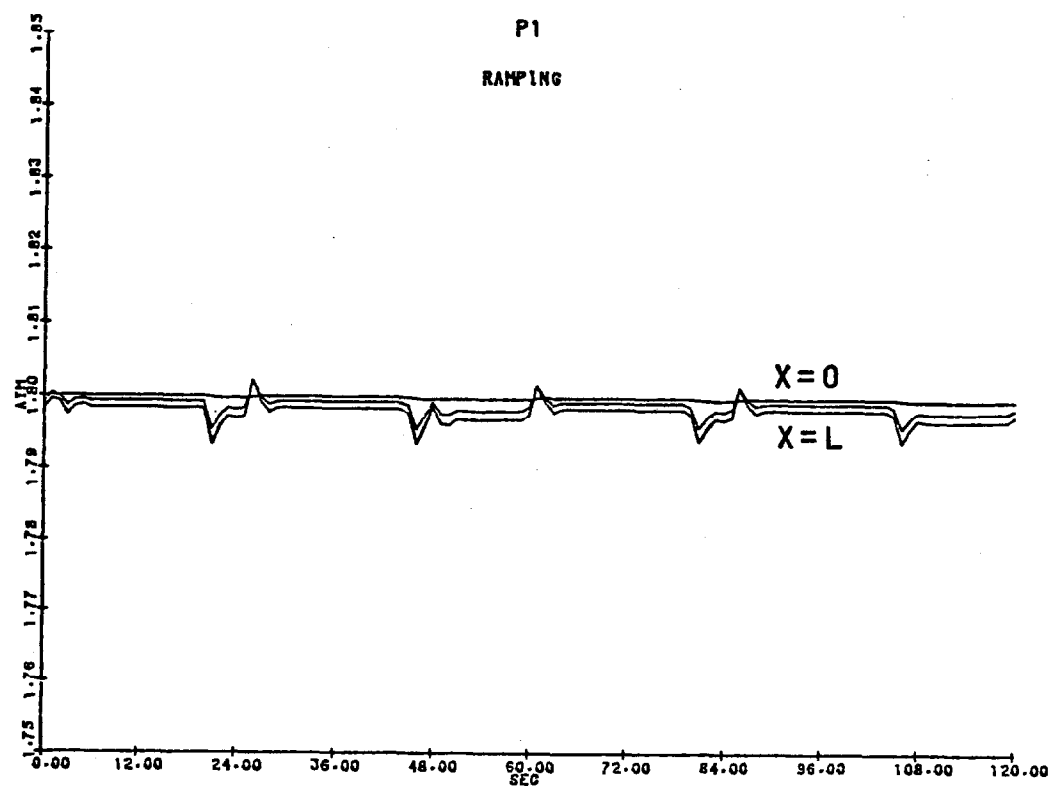
Figure 16. Pressure of single-phase stream over two ramp cycles.
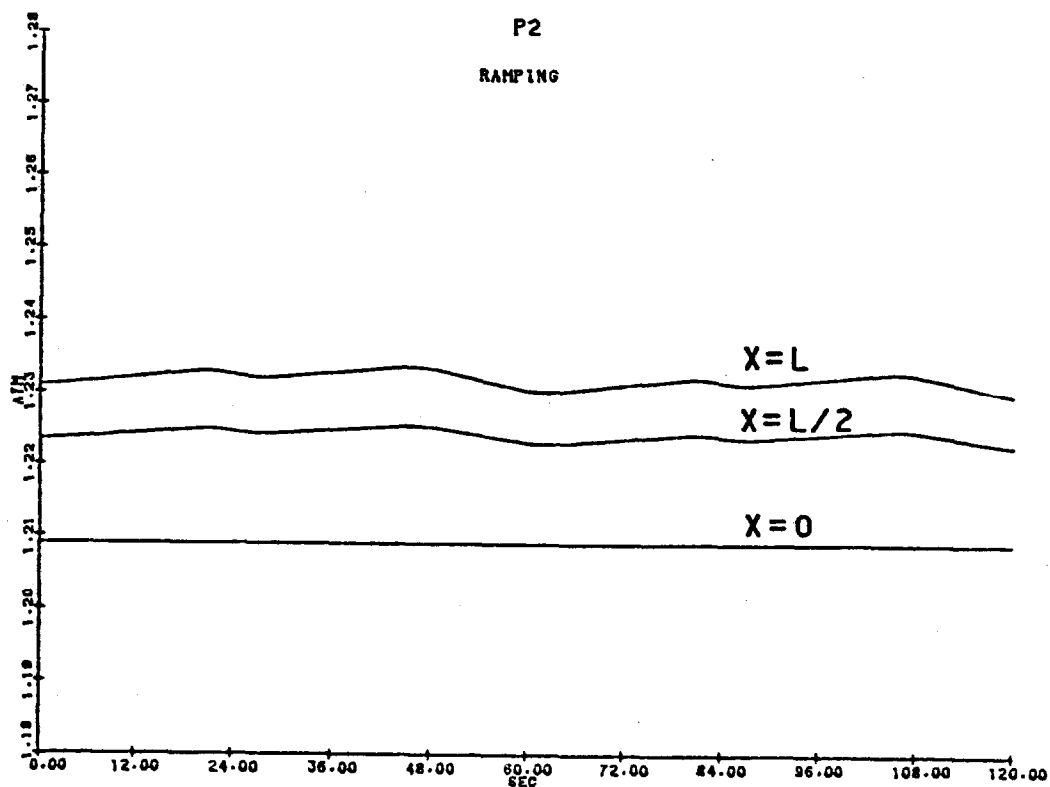
Figure 17. Pressure of two-phase stream over two ramp cycles.
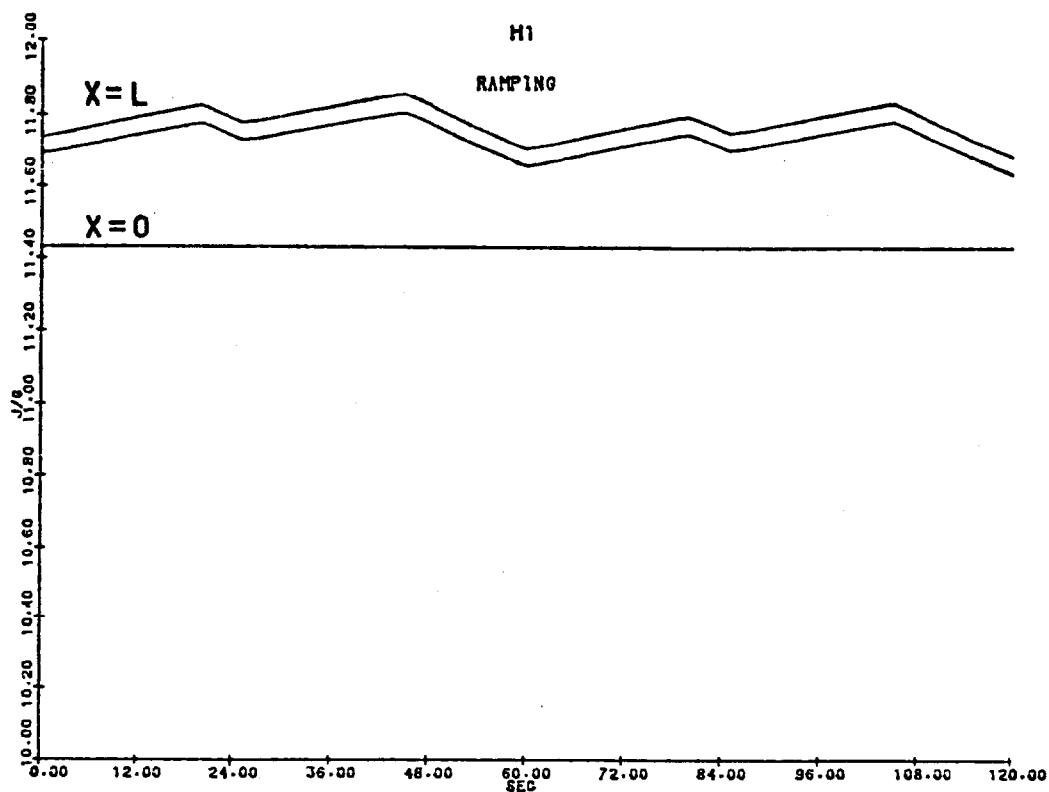
Figure 18.   Enthalpy of single-phase stream over two ramp cycles.
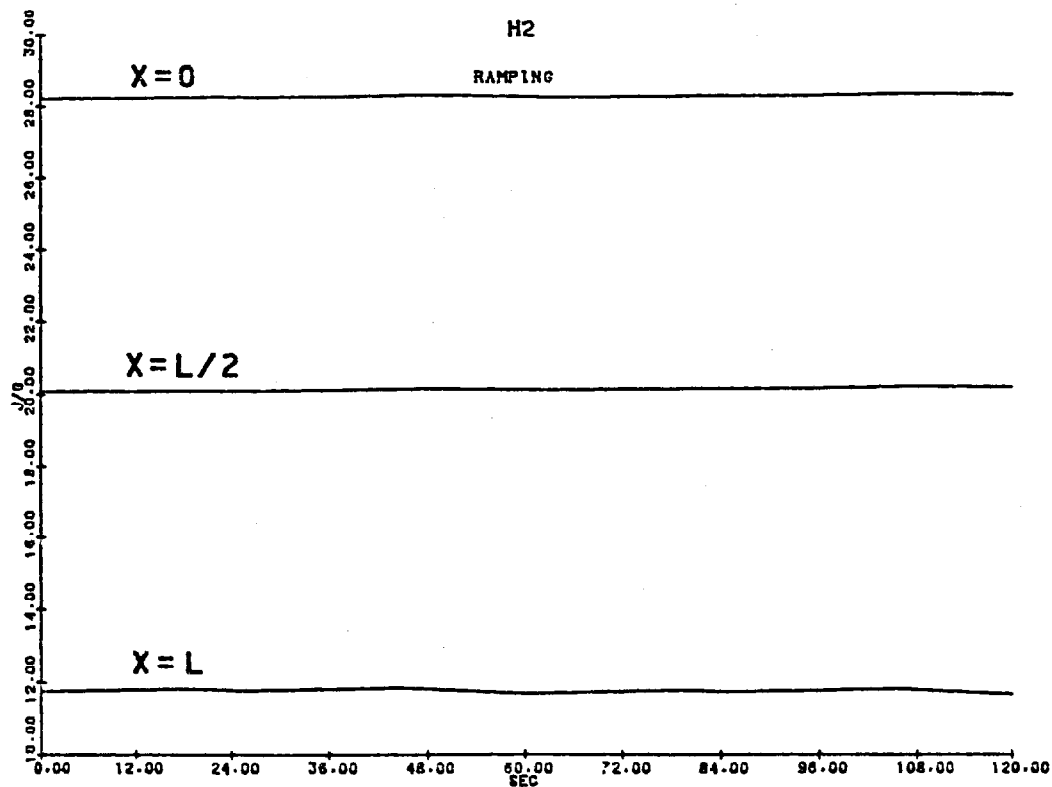
Figure 19.   Enthalpy of two-phase stream over two ramp cycles.
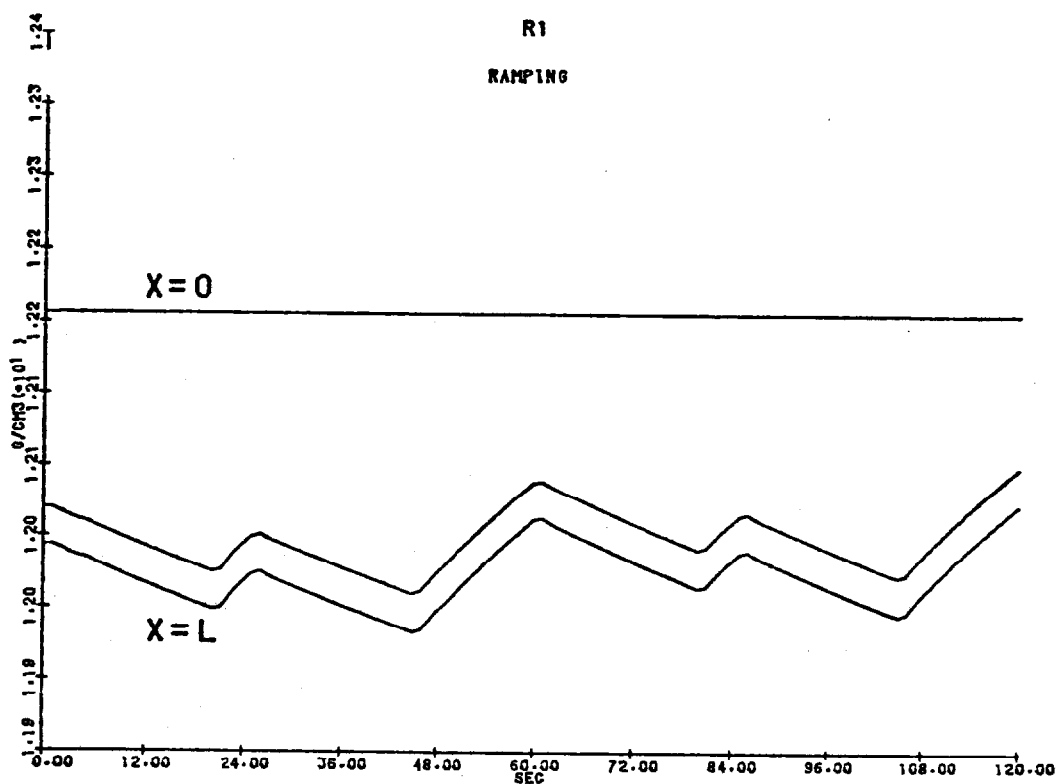
Figure 20. Density of single-phase stream over two ramp cycles.
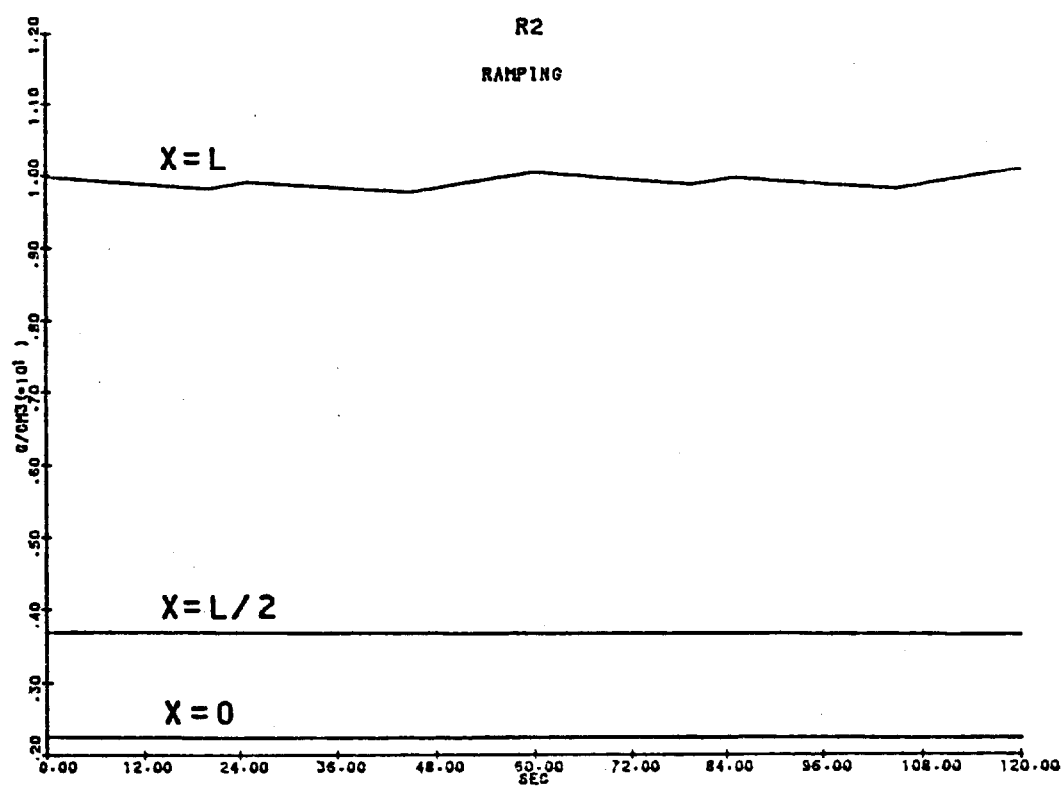
Figure 21. Density of two-phase stream over two ramp cycles.
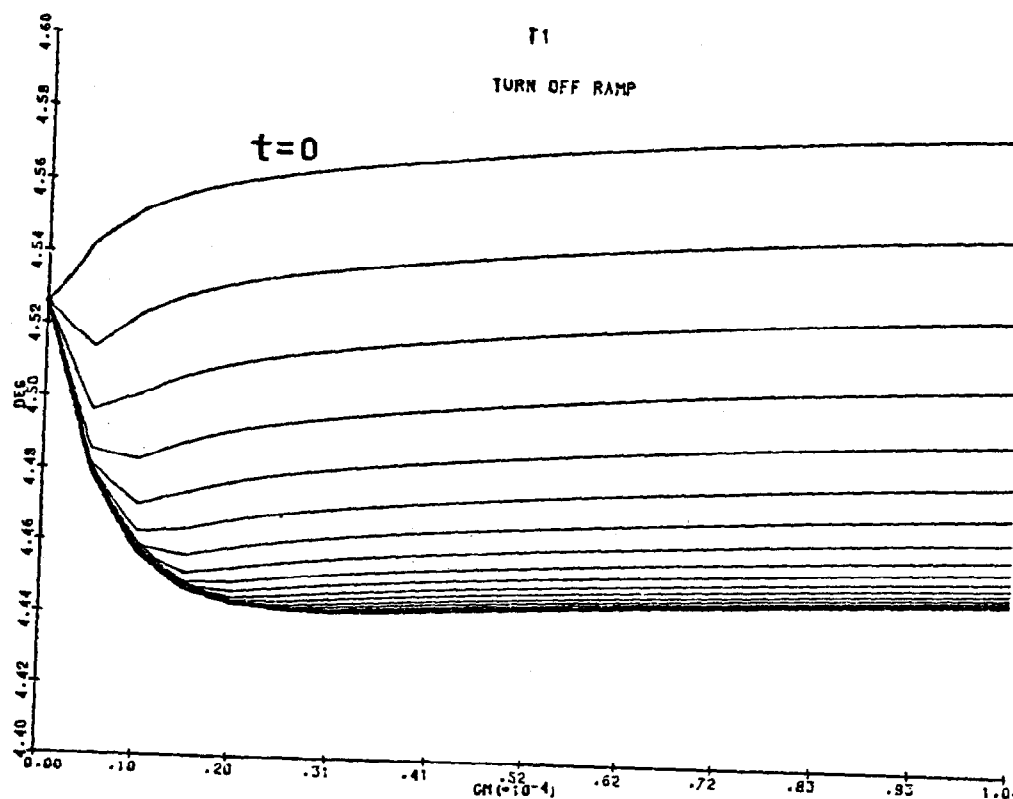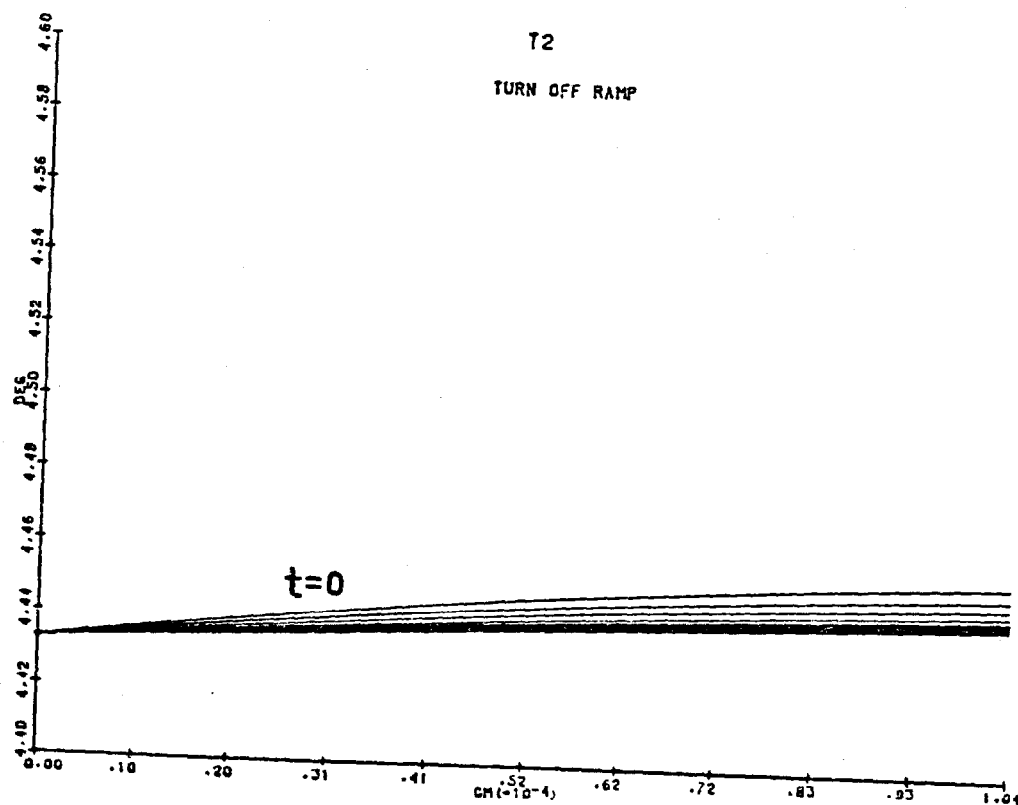
Figure 24.   Pressure of single-phase stream as a function of x at
             20 sec intervals.
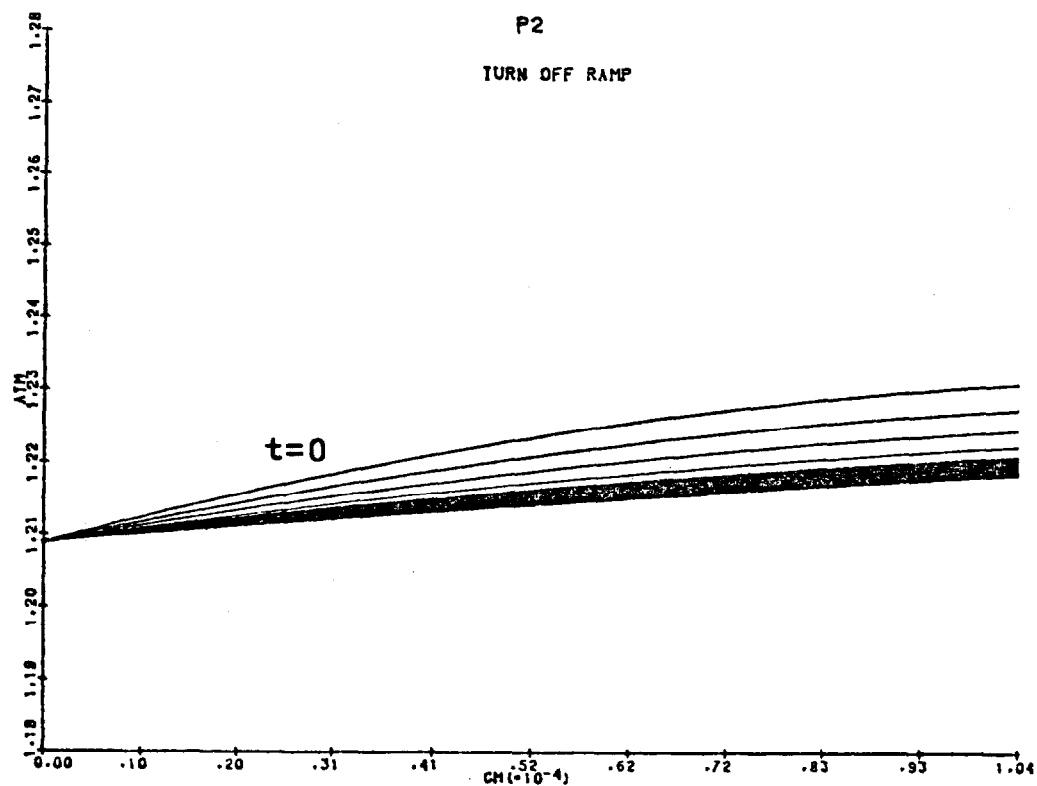
Figure 25.   Pressure of two-phase stream as a function of x at
             20 sec intervals.
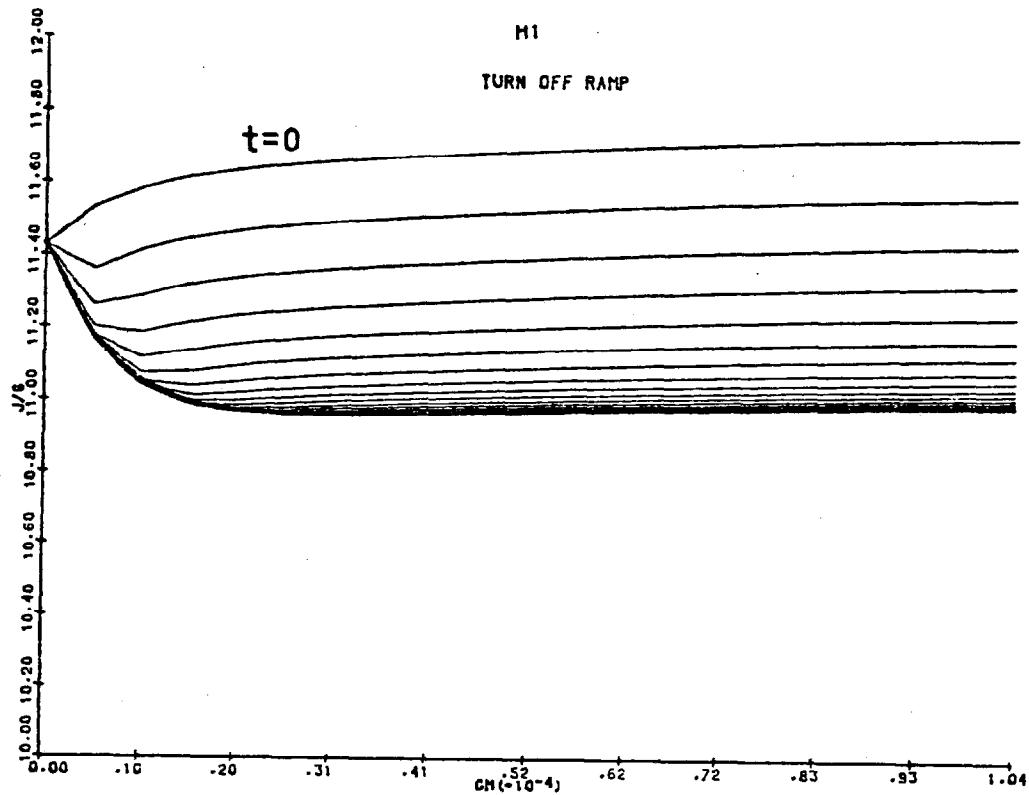
Figure 26.   Enthalpy of single-phase stream as a function of x
             at 20 sec entervals.
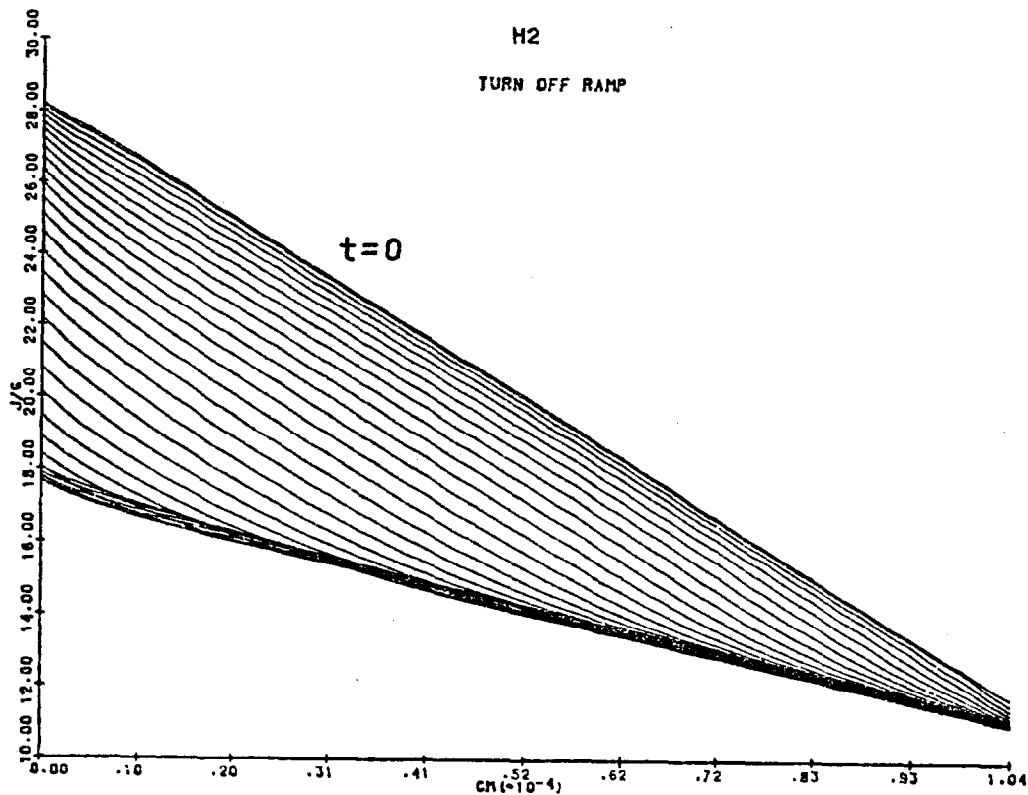
Figure 27.   Enthalpy of two-phase stream as a function of x at
             20 sec intervals.

Figure 28.   Velocity of single-phase stream as a function of x at
             20 sec intervals.

Figure 29.   Velocity of two-phase stream as a function of x at
             20 sec intervals.
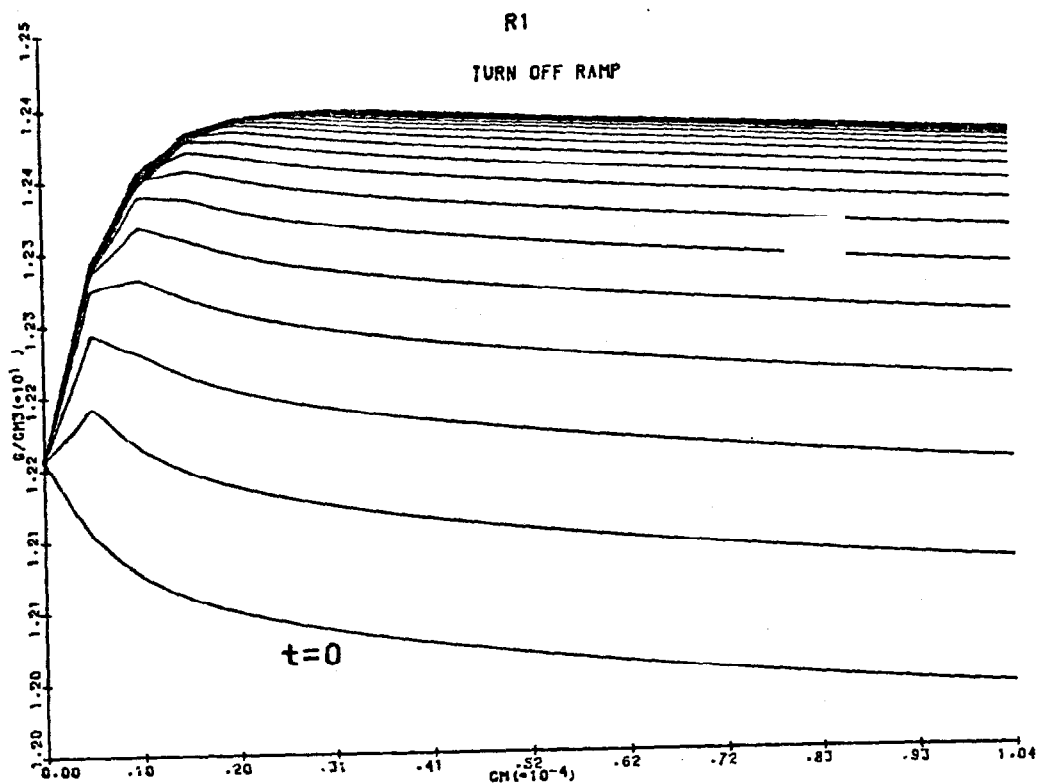
Figure 30.   Density of single-phase stream as a function of x at
             20 sec intervals.
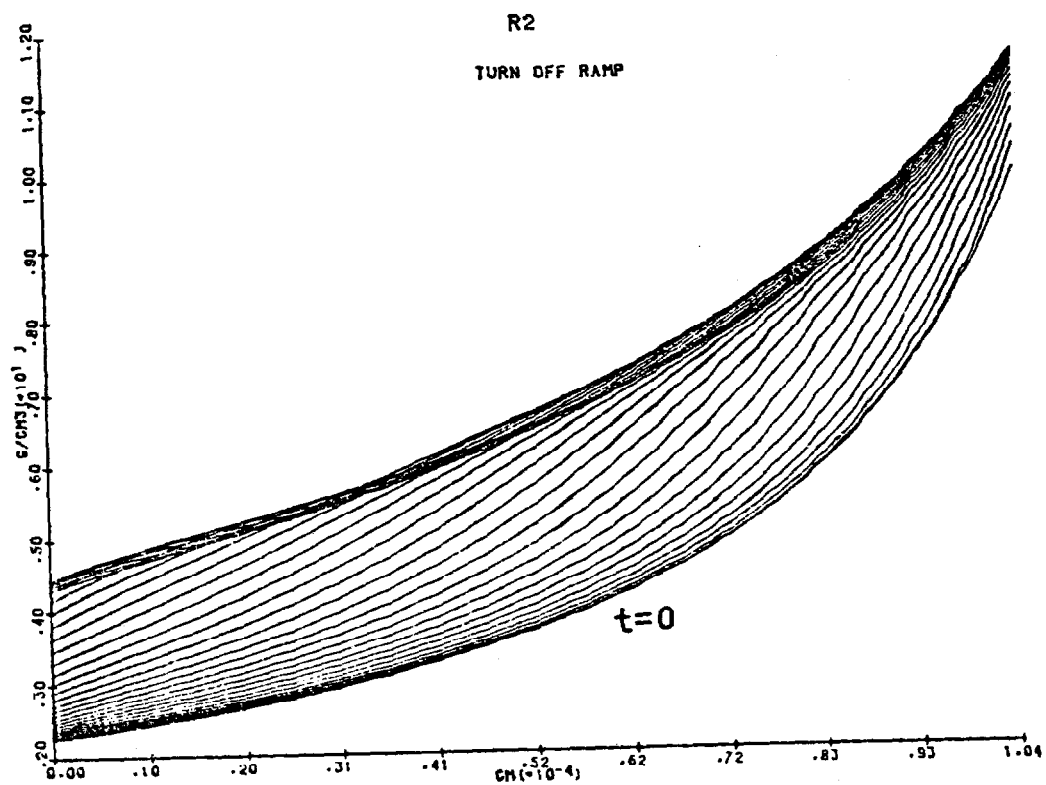
Figure 31.   Density of two-phase stream as a function of x at 20
             sec intervals.
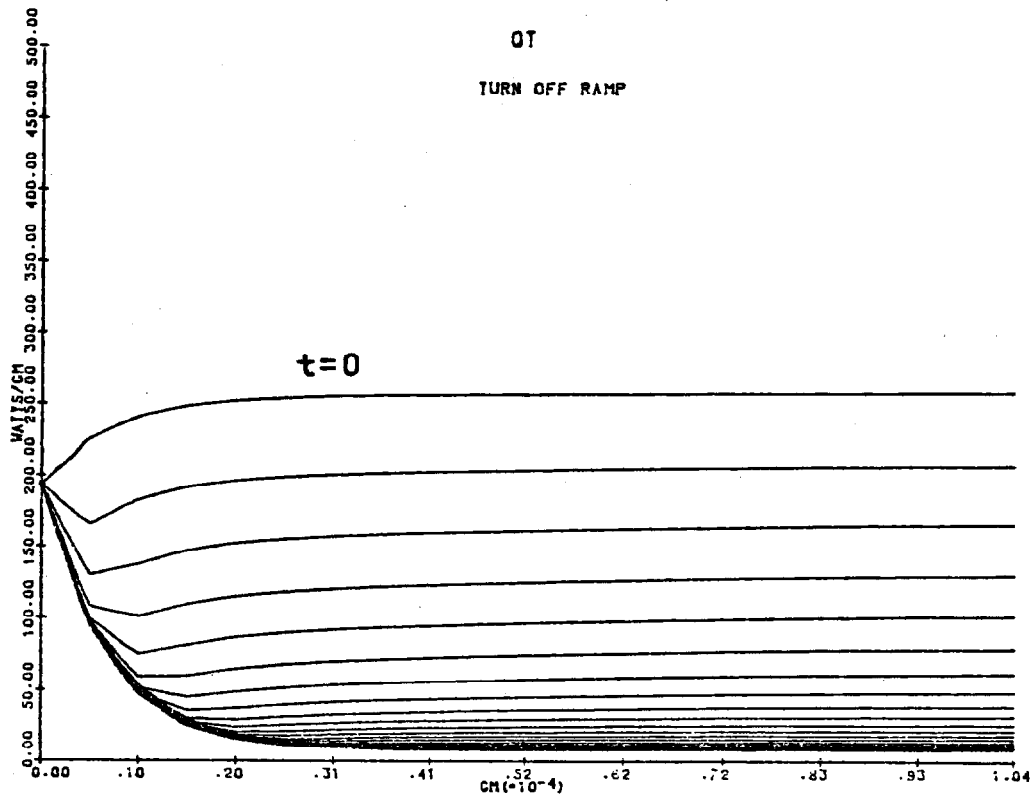
Figure 32.   Heat transfer as a function of x at 20 sec intervals.
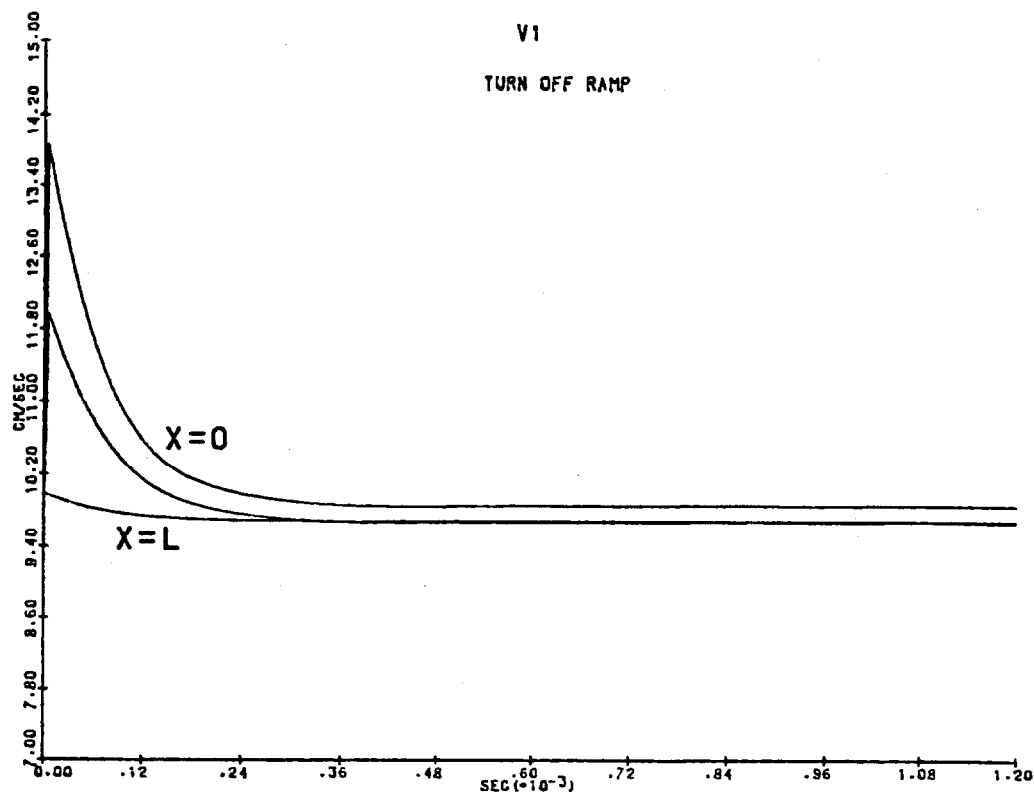
Figure 33. Velocity of single-phase stream as a function of time at x=0, L/2, and L.
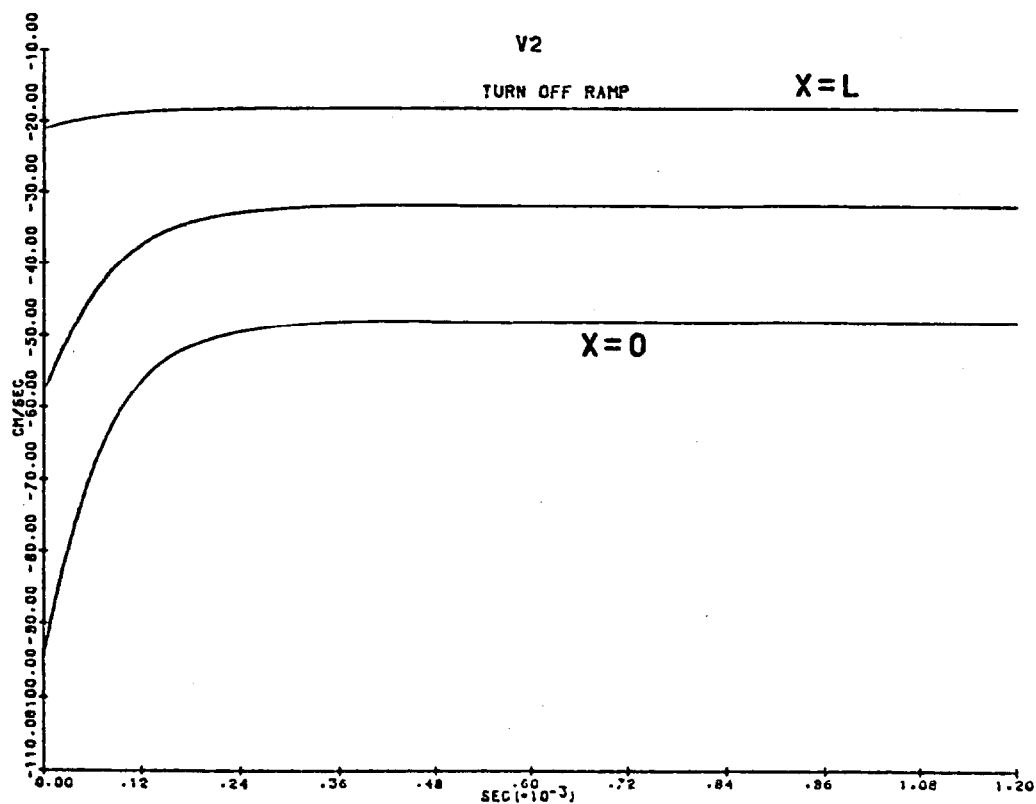
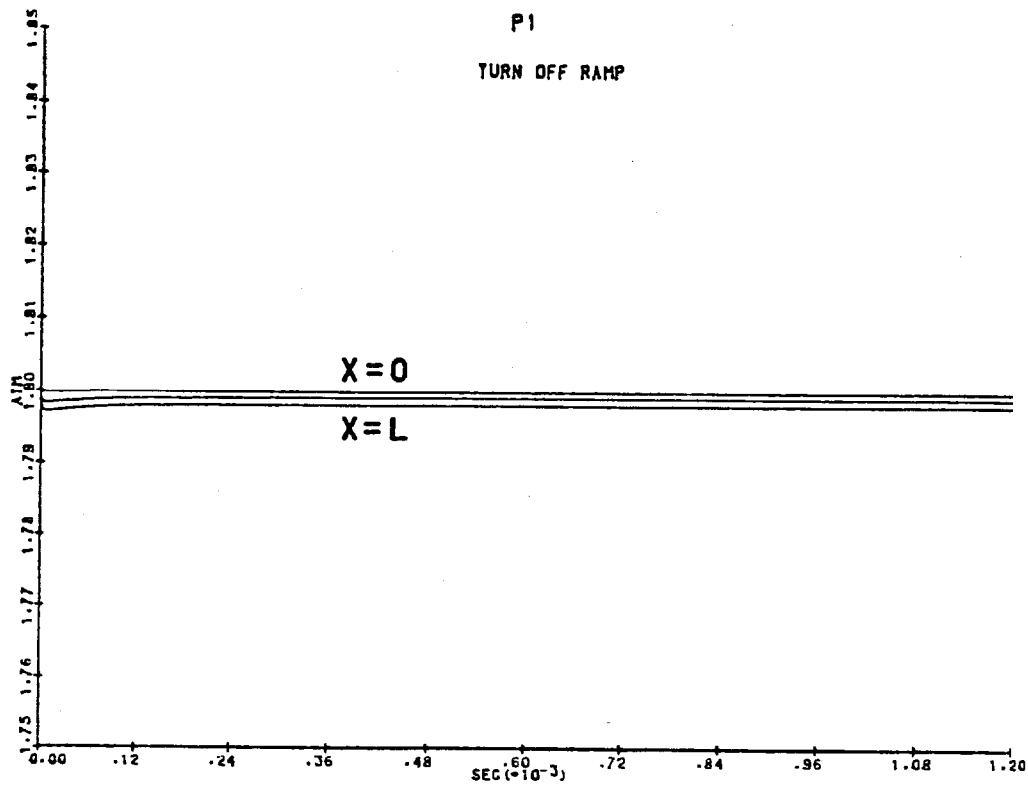Figure 34. Velocity of two-phase stream as a function of time at x=0, L/2, and L.
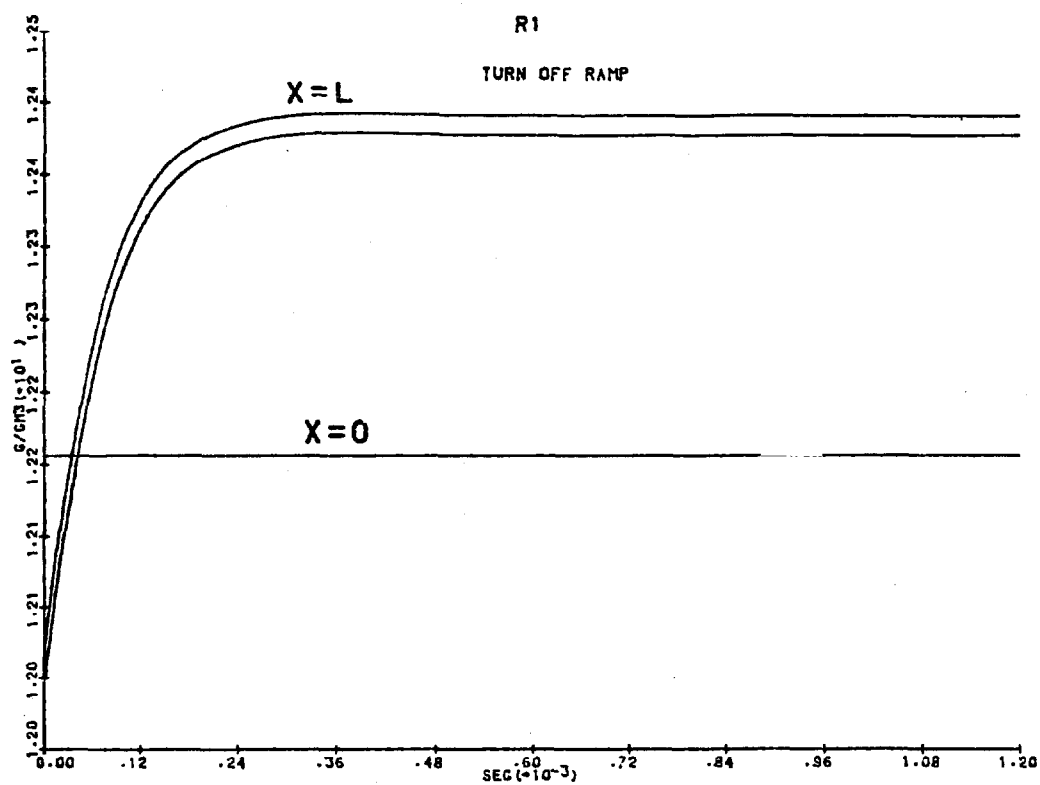
Figure 35.   Density of single-phase stream as a function of time
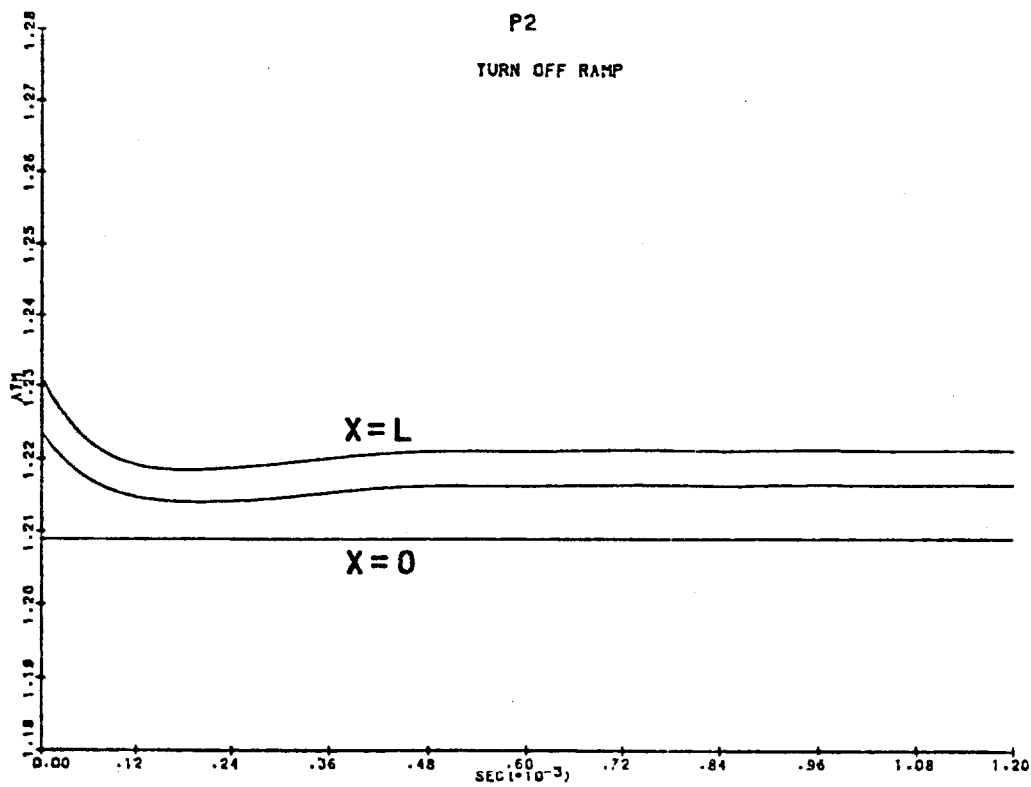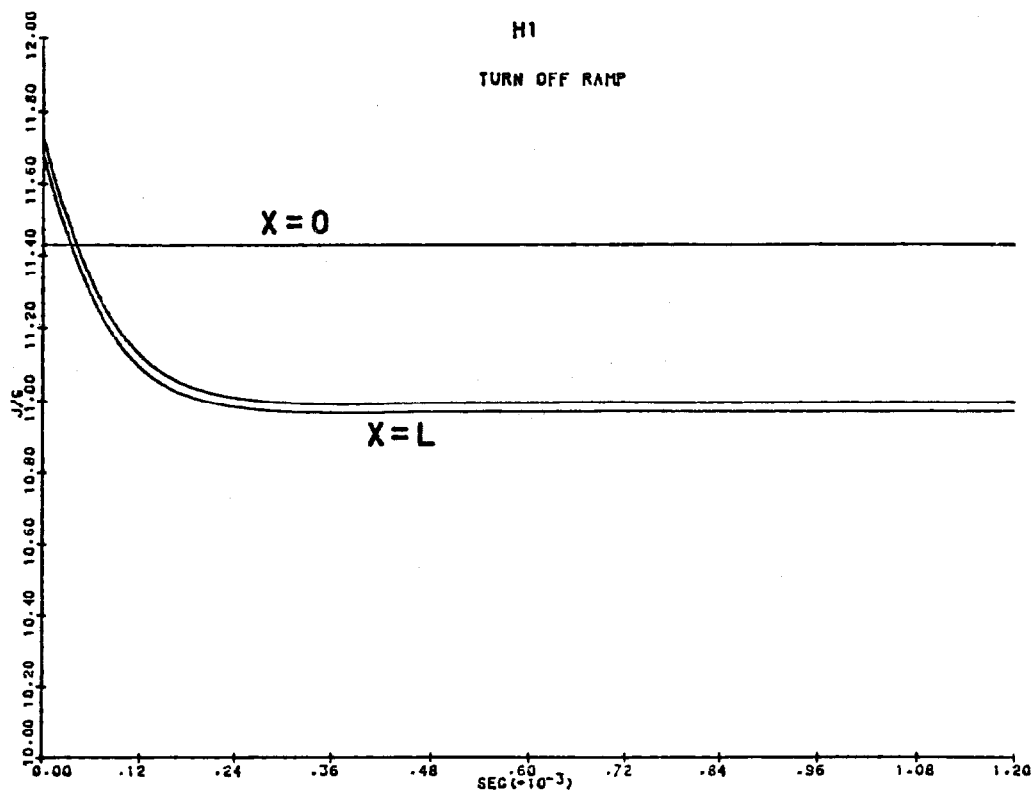   at x=0, L/2, and L.
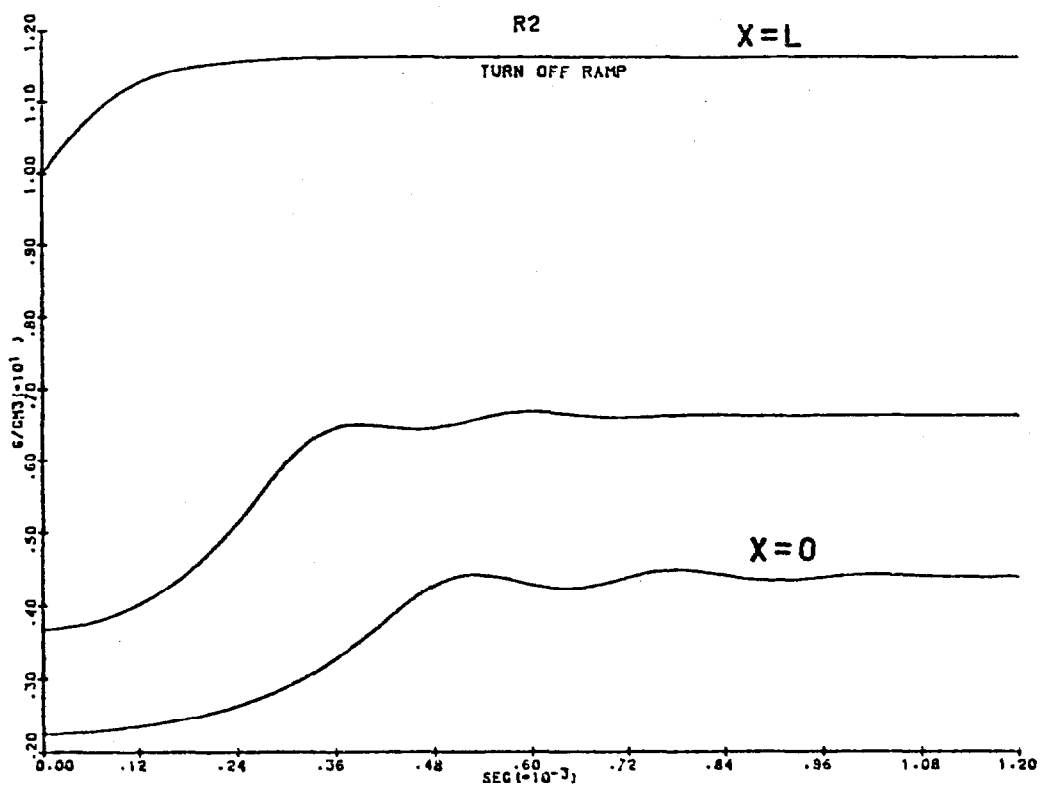
Figure 36.   Density of two-phase stream as a function of time at
             x=0, L/2, and L.

Figure 37. Pressure of single-phase stream as a function of
time at x=0, L/2, and L.

Figure 38.   Pressure of two-phase stream as a function of time
at x=0, L/2, and L.

Figure 39.   Enthalpy of single-phase stream as a function of
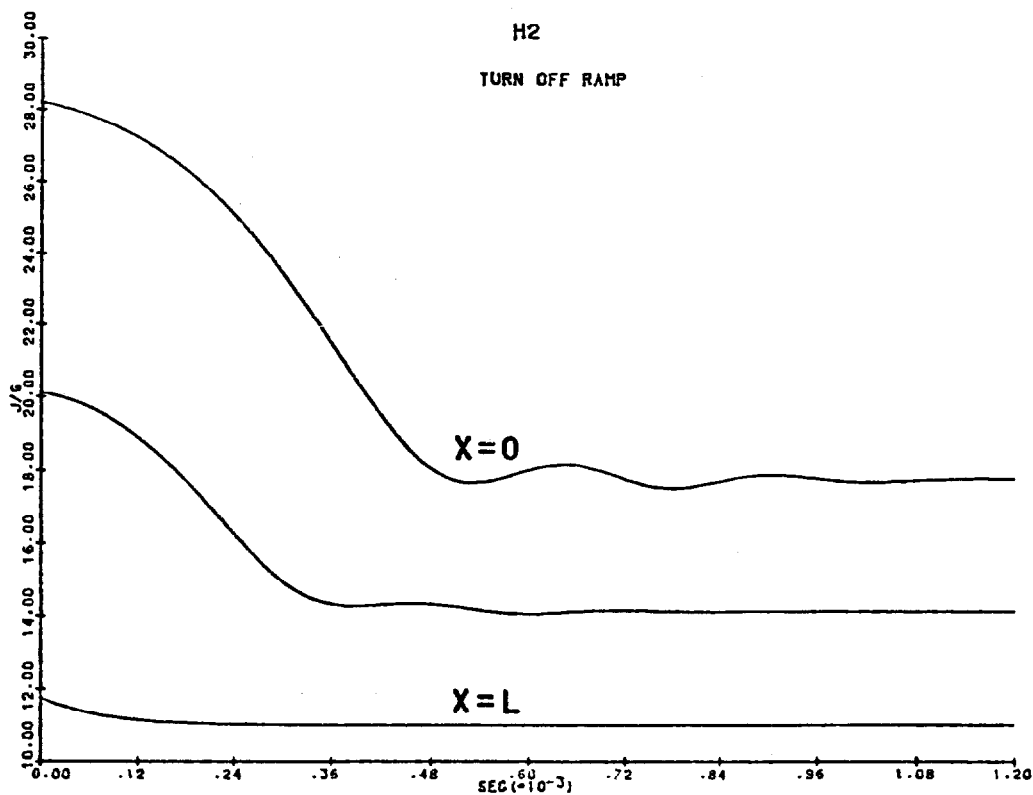   time at x=0, L/2, and L.

Figure 40.   Enthalpy of two-phase stream as a function of time
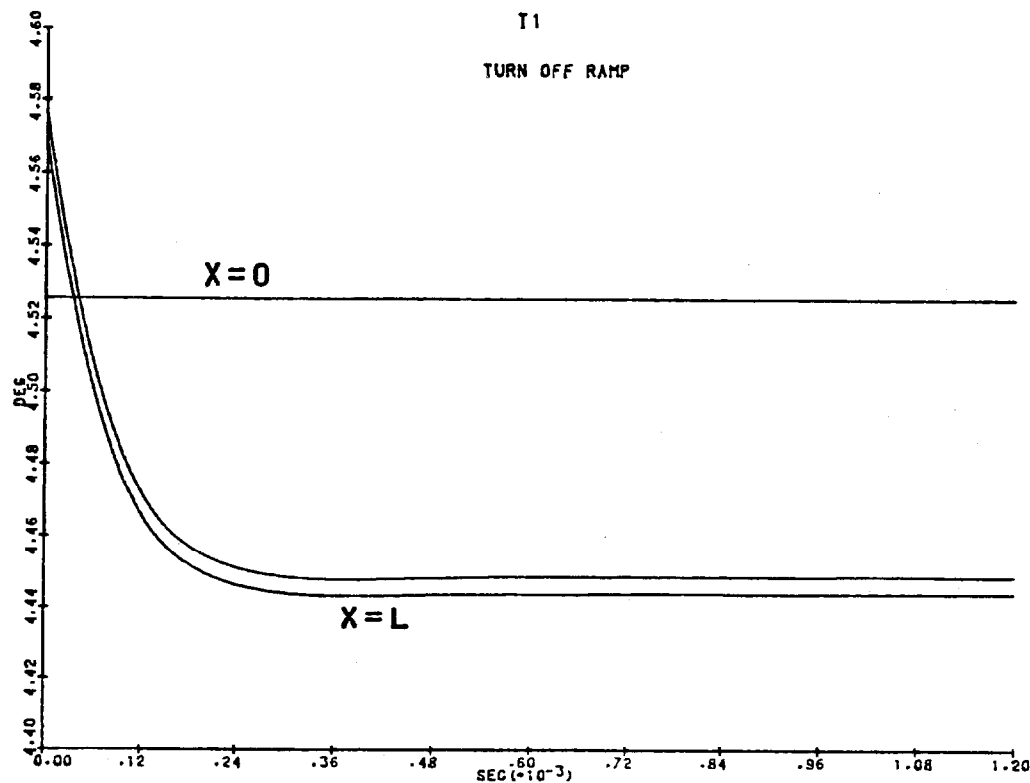   at x=0, L/2, and L.

Figure 41.   Temperature of single-phase stream as a function of
time at x=0, L/2, and L.
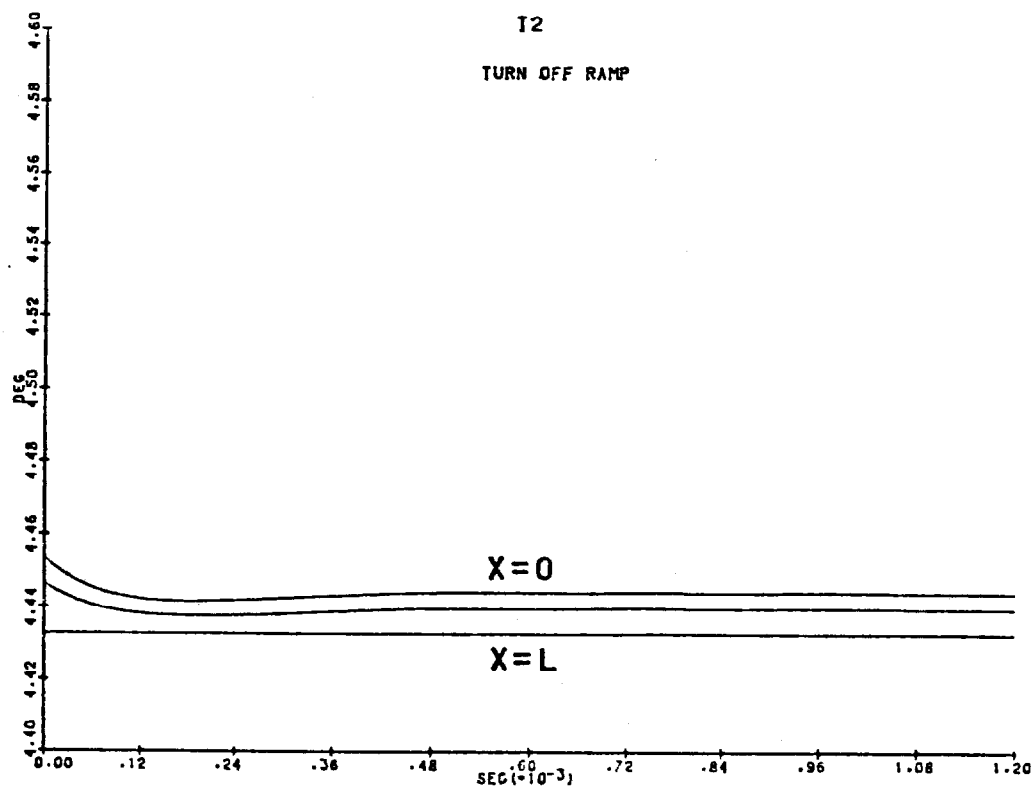

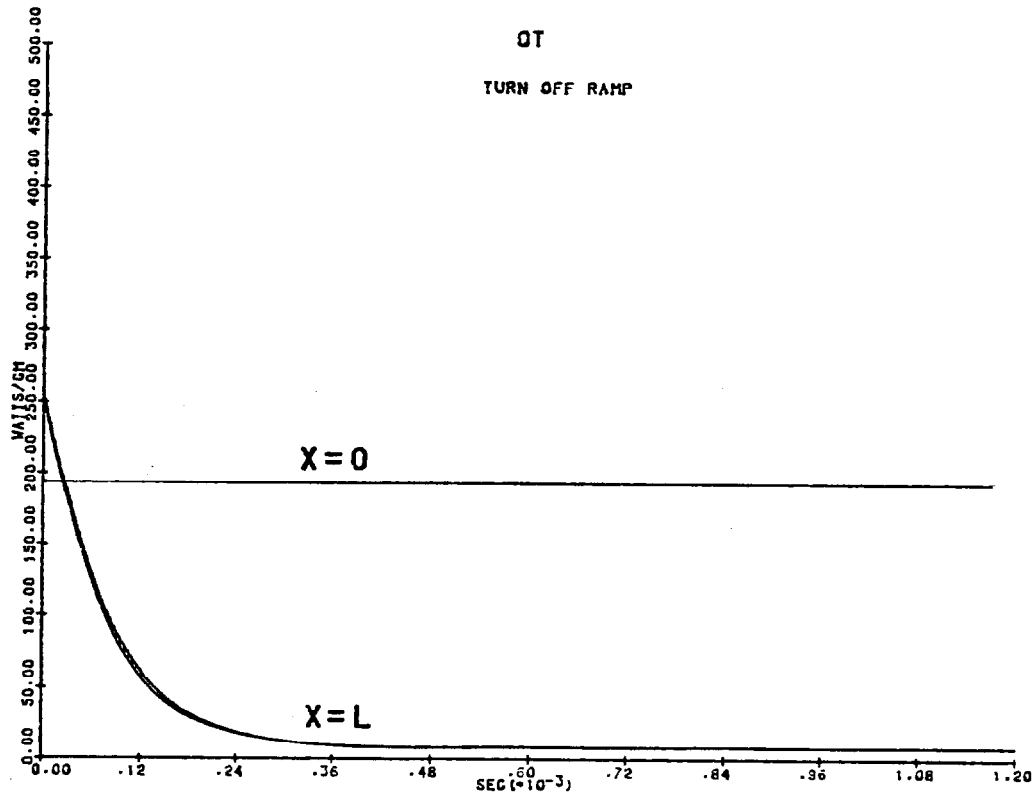Figure 42.   Temperature of two-phase stream as a function of
time at x=0, L/2, and L.

Figure 43.   Heat transfer as a function of time at x=0, L/2, and
              L.